European Journal of Medicinal Chemistry Reports 12 (2024) 100183

Contents lists available at ScienceDirect

European Journal of Medicinal Chemistry Reports

journal homepage: www.editorialmanager.com/ejmcr/default.aspx

Thiadiazole-thiazole derivatives as potent anti-tubercular agents: Synthesis, biological evaluation, and *In silico* docking studies

Samin A. Shaikh [a,d,*], Shivaji R. Labhade [a], Raju R. Kale [a], Prajakta Y. Pachorkar [b], Rohan J. Meshram [c], Kamlesh S. Jain [d], Hrishikesh S. Labhade [a], Dipak D. Bhanushali [d], Rahul A. More [e], Charushila K. Nerkar [f], Santosh S. Chobe [f], Aniket N. Marathe [c], Satish N. Wakchaure [g], Deepak R. Boraste [h]

[a] *Department of Chemistry, KTHM College, Gangapur Road, Nashik, Maharashtra, India*
[b] *Department of Microbiology, KTHM College, Gangapur Road, Nashik, Maharashtra, India*
[c] *Bioinformatics Centre, Savitribai Phule Pune University, Pune, Maharashtra, India*
[d] *Department of Chemistry, Kr. V. N. Naik Shikshan Prasarak Sanstha's Arts, Commerce and Science College, Canada Corner, Nashik, Maharashtra, India*
[e] *Department of Microbiology, Dayanand Science College, Latur, Maharashtra, India*
[f] *Department of Chemistry, M.G. V's Loknete Vyankatrao Hiray, Arts, Science and Commerce College, Panchavati, Nashik, Maharashtra, India*
[g] *Department of Synthetic R & D, Delta Finochem Private Limited, Gat No. 350, Village Wadivarhe, Tal-Igatpuri, Nashik, Maharashtra, India*
[h] *G. E. Society's, R.N.C Arts, J.D.B Commerce, and N.S.C. Science College, Nashik Road, Nashik, 422101, Maharashtra, India*

ARTICLE INFO

Keywords:
Anti-tuberculosis
Thiazole
Tetra-n-butylammonium bromide
Thiadiazole

ABSTRACT

The present study focuses on research findings related to the development and assessment of thiadiazole-linked thiazole derivatives as promising anti-tubercular agents. We present the synthesis data of eleven new compounds (**4a-4k**) and confirm their structures using spectroscopic techniques. Subsequently, the compounds were screened for their anti-tuberculosis activities against *M. tuberculosis* H37Ra. The results demonstrated that compounds **3** and **4b** exhibited minimum inhibitory concentration (MIC) of **3.90 μg/mL** and **7.81 μg/mL**, respectively. *In-vitro*, studies for few compounds exhibited high antioxidant activity against DPPH and OH radical scavengers along with minimal to no cytotoxicity against RBCs which is a promising result. Investigation of molecular docked conformations revealed different molecular interactions such as hydrogen bonds, halogen bonds, and interactions involving Pi electron cloud. The study sheds light on conserved interactions with residues like Met131, Val163, His90 and Gln161 from the tubercular MCAT enzyme. Interestingly, the synthetic chemistry reveals that the employment of tetra-n-butylammonium bromide (TBAB) plays a crucial role for N-butylation and it also expedites the reaction in tetrahydrofuran solvent.

1. Introduction

According to the World Health Organization (WHO) in its recent report (2021), tuberculosis (TB) remains one of the top ten causes that is responsible for the global deaths. Specifically, it poses a grave threat to the developing and underdeveloped countries worldwide [1]. To eradicate TB, the use of first-line standard drugs such as isoniazid, rifampicin, delamanid, bedaquiline, ethambutol, and pyrazinamide (Fig. 1) has witnessed limited success. In addition to their therapeutic action, the above drugs also exhibit some toxic side effects, such as QT prolongation, CNS toxicity, and hepatotoxicity [2]. To overcome these limitations, recent research has approved a combination therapy of bedaquiline and linezolid to treat adult patients suffering from multidrug-resistant tuberculosis (MDR-TB) and extensive drug-resistant tuberculosis (XDR-TB) [3]. It was observed that around 81 % of the patients with peripheral neuropathy undergoing the above treatment showed hematologic toxic effects. The increases in tuberculosis cases can be directly linked to the emergence of MDR-TB and XDR-TB [4]. Eradicating tuberculosis by 2050 to a greater extent is one of the major goals of WHO [5]. In view of the development of MDR-TB and XDR-TB there is an urgent need and demand to find new anti-tuberculosis drugs that are efficacious and safe [6].

Thiazoles are 5-membered heterocyclic compounds that contain both nitrogen and sulfur atoms. Numerous thiazole derivatives exhibit a

* Corresponding author. Department of Chemistry, KTHM College, Gangapur Road, Nashik, Maharashtra, India.
E-mail address: saminshaikh80@gmail.com (S.A. Shaikh).

https://doi.org/10.1016/j.ejmcr.2024.100183
Received 31 March 2024; Received in revised form 10 June 2024; Accepted 24 June 2024
Available online 27 June 2024

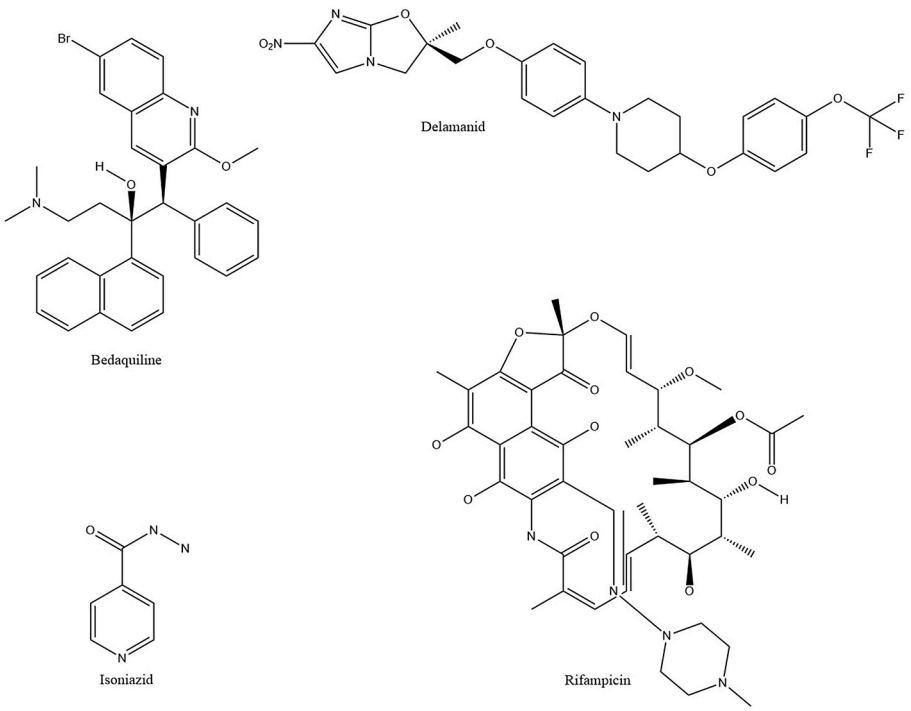

Fig. 1. Chemical structures of few commercially available antituberculosis drugs.

broad range of biological activities, including anticancer [7], antituberculosis [8], antibacterial [9], antiinflammatory [10], antiviral [11], antimicrobial [12], ecto-50-nucleotidase inhibitors [13], and many more. Interestingly, the 1,3,4-thiadiazole molecule that compromises of a sulfur pharmacophore is a vital scaffold in medicinal chemistry that exhibits biological activities such as antibacterial [14], lysine acetyl-transferase inhibitor [15], anticonvulsant [16], antitumor [17], antioxidant [18] etc. Considering the properties exhibited by the thiadiazole moiety herein we have designed, synthesized, and evaluated the antitubercular, antioxidant and non-cytotoxic activities of 11 novel molecular hybrids of thiazole-1,3,4-thiadiazoles clubbed through alpha-thio amide linkage. (**4a-4k**). Fig. 2 below depicts few thiazoles and thiadiazole drugs and a strategy to combine the core moieties to obtain novel thiazole-thiadiazole derivatives intended for evaluating their antituberculosis activities. Performing these, antioxidant assays is crucial because oxidative stress has been implicated in the pathogenesis of tuberculosis [19]. Reactive oxygen species (ROS) and reactive nitrogen species (RNS) are produced during the host's immune response to *M. tuberculosis* infection, potentially leading to tissue damage and contributing to disease progression [20].

Antioxidant compounds can mitigate this oxidative stress, thereby providing an additional therapeutic benefit. Therefore, assessing the antioxidant activity of these derivatives complements their antimicrobial evaluation, offering insights into their potential dual role in TB therapy.

Conducting haemolytic assays is essential to ensure the safety and biocompatibility of the synthesized compounds alongside their efficacy [21]. While evaluating the antitubercular and antioxidant activities of screened compounds is crucial for determining their potential as therapeutic agents against tuberculosis, assessing their cytotoxicity, particularly their impact on red blood cells (RBCs) is equally important. Haemolytic assays help determine whether screened compounds cause haemolysis, which is the destruction of RBCs, leading to the release of haemoglobin into the bloodstream [22]. This is a critical step, as a compound with high antioxidant activity but significant haemolytic activity would pose a risk to the patient, potentially causing anaemia or other serious side effects. Therefore, the haemolytic assays provide a comprehensive evaluation of the therapeutic index of these compounds, balancing their efficacy against *Mycobacterium tuberculosis* and oxidative stress with their safety profile, ensuring that they do not adversely affect the host's RBCs [23]. This holistic approach in the evaluation process helps in identifying promising candidates that are both effective and safe for further development in the treatment of tuberculosis. Moreover, molecular docking studies were conducted to elucidate their binding interactions with the target proteins. This multifaceted approach not only highlights the therapeutic potential of these thiazole-thiadiazole derivatives but also provides insights into their mechanism of action, paving the way for further optimization and development.

2. Experimental

*2.1. General procedures for synthesis of thiazole based acetamide derivatives (**2a-2k**) [24]*

The mixture of thiazol-2-amino derivatives **1a-1k** (1.0 mmol) and triethylamine (1.3 mmol) was taken in a round-bottom flask. The reaction mass was stirred at room temperature for 30 min. Chloroacetyl chloride (CAC) (2.2 mmol) was added to reaction mass at 0–5 °C. The reaction was completed within 1–4 h as monitored by thin layer chromatography. After the reaction completion the products were filtered and washed with water. Mobile phase: n-hexane: ethyl acetate (6:4).

*2.2. General procedure for synthesis of 5-amino-1,3,4-thiadiazole-2-thiol (**3**) [25]*

A mixture of thiosemicarbazide (10.0 mmol), anhydrous Na_2CO_3 (10.0 mmol) and carbon disulfide (10.0 mmol) was suspended in absolute ethanol. The reaction mixture was refluxed for 8 h. The solvent was evaporated under vacuum and the residue was dissolved in water (20 mL) and acidified with conc. HCl to yield compound **3** (84 %).

*2.2.1. 5-amino-1,3,4-thiadiazole-2-thiol (**3**)*

m. p. 232 °C, yield: 78 %, brown powder, ^{1}**H-NMR** (500 MHz, DMSO-d_6): δ 4.51 (s, 2H), 9.94 (s, 1H). ^{13}**C-NMR** (126 MHz, DMSO-d_6):

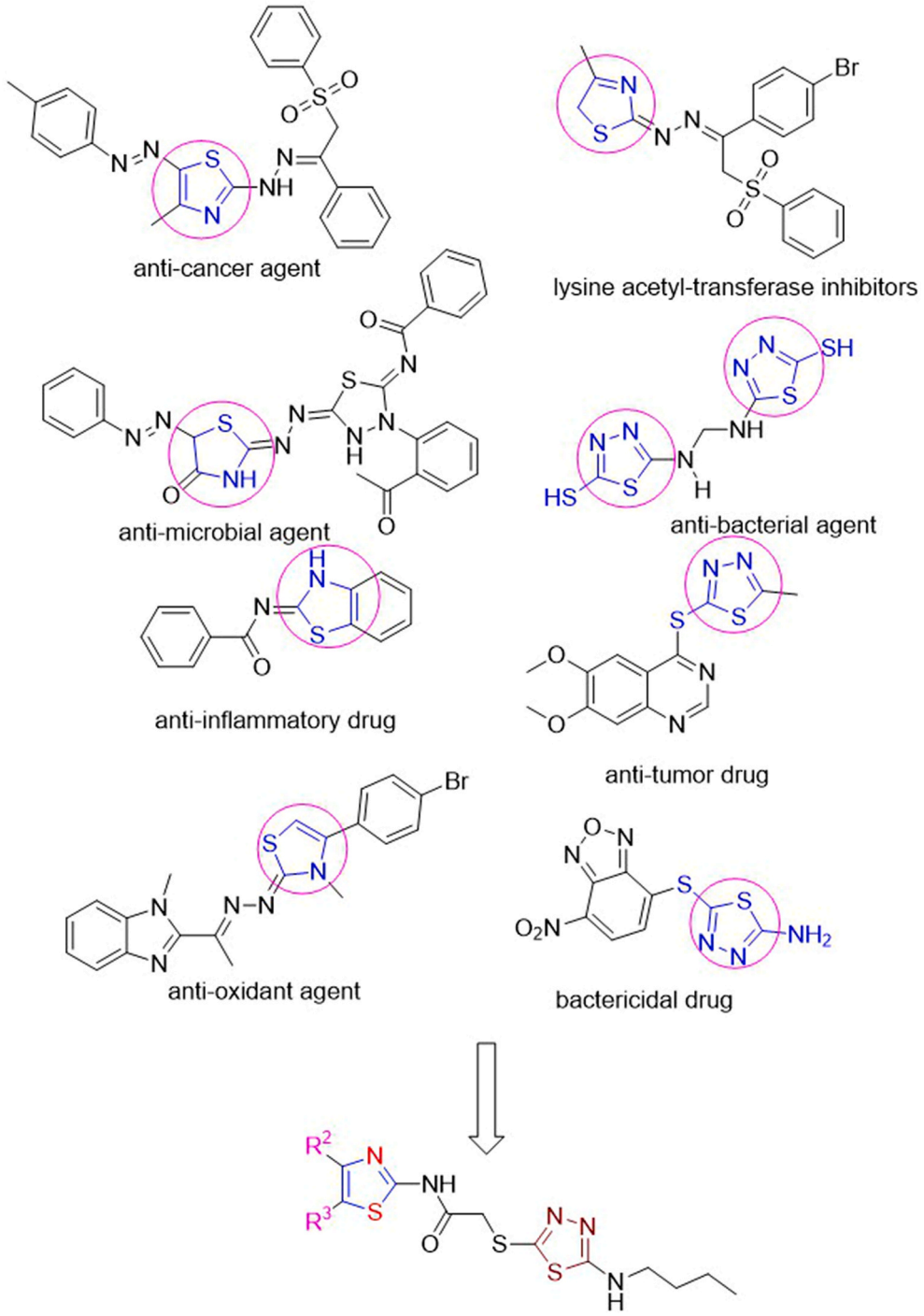

Fig. 2. Synthetic strategy to obtain thiazole-thiadiazole derivatives.

δ 140.66,157.80.

*2.3. General procedures for the synthesis of 2-((5-(Butylamino)-1,3,4-thiadiazol-2-yl)thio)-N-(thiazol-2-yl)acetamide derivatives (**4a-4k**)*

A solution of 5-amino-1,3,4-thiadiazole-2-thiol (**3**) (1 mmol) and anhydrous K_2CO_3 (1.1 mmol) in THF (10 mL) was stirred at ambient temperature for 30 min. Subsequently, the solution of **thiazole based acetamide derivatives** (**2a-2k**) (1 mmol) and tetra butyl ammonium bromide (TBAB) (1.1 mmol) in THF (10 mL) was added dropwise through dropping funnel to the reaction mass. Stirred the reaction mass at room temperature and monitored the reaction progress by TLC. After the reaction completion, the mixture was poured onto crushed ice. Crude product precipitates out which was filtered, washed with brine solution, and recrystallized from ethyl acetate to obtain pure product. Mobile phase: toluene: ethyl acetate: acetic acid (5:4:1).

*2.3.1. 2-((5-(butylamino)-1,3,4-thiadiazol-2-yl)thio)-N-(4-phenylthiazol-2-yl) acetamide (**4a**)*

m.p. 218–220 °C, yield: 89 %, brown powder; FT IR: 620, 1178, 1335, 1510, 1616, 3475 cm^{-1}; Elemental Analysis calc %: C, 45.32; H, 4.03; N, 18.65; O, 10.65; S, 21.35; **^{1}H-NMR** (500 MHz, DMSO-d_6): ppm 0.93 (t, $J = 7.3$ Hz, 3H), 1.31 (sextet, $J = 7.3$ Hz, 2H), 1.60 (m, 2H), 3.10 (m, 2H), 4.11 (s, 2H), 7.46–7.31 (m, 3H), 7.66 (s, 1H), 7.56 (s, 1H), 7.90

(dd, J = 6Hz, 3.3 Hz, 2H), 12.53 (s, 1H); **^{13}C-NMR** (126 MHz, DMSO-d_6): δ 13.59, 19.36, 23.27, 37.28, 57.69, 108.44, 125.69 (strong), 127.86, 128.50 (strong), 134.23, 148.55, 148.84, 157.51, 166.46, 170.47; $C_{17}H_{19}N_5OS_3$, Exact Mass: 405.55; Observed Mass (M + 1): 407.

*2.3.2. N-(4-(4-bromophenyl)thiazol-2-yl)-2-((5-(butylamino)-1,3,4-thiadiazol-2-yl)thio) acetamide **(4b)***

m.p. 278–280 °C, yield: 86 %, brown powder; FT IR: 620, 1177, 1383, 1516, 1617, 3470 cm^{-1}; Elemental analysis calc %: C, 42.15; H, 3.75; Br, 16.49; N, 14.46; O, 3.30; S, 19.85; **^{1}H-NMR** (500 MHz, DMSO-d_6): δ 0.87 (t, J = 7.3 Hz, 3H), 1.26 (sextet, J = 7.2 Hz, 2H), 1.51 (quintet, J = 15.5, 8.0 Hz, 2H), 3.14 (t, 2H), 4.05 (s, 2H), 7.26 (s, 1H), 7.57 (d, J = 8.5 Hz, 2H), 7.67 (s, 1H), 7.79 (d, J = 8.5 Hz, 2H), 12.49 (s, 1H); **^{13}C-NMR** (126 MHz, DMSO-d_6): δ 13.36, 19.09, 22.94, 37.17, 57.42, 109.08, 120.80, 127.58 (strong), 131.58 (strong), 133.27, 147.64, 148.65, 157.71, 166.46, 170.00; $C_{17}H_{18}BrN_5OS_3$, Exact Mass: 484.98; Observed Mass (M + 2): 487.

*2.3.3. 2-((5-(butylamino)-1,3,4-thiadiazol-2-yl)thio)-N-(4-(4-chlorophenyl)thiazol-2-yl) acetamide **(4c)***

m.p. 208–210 °C, yield: 90 %, brown powder; FT IR: 620, 744, 1181, 1385, 1502, 1617, 3476 cm^{-1}; Elemental analysis calc %: C, 46.41; H, 4.12; Cl, 8.06; N, 15.92; O, 3.64; S, 21.86; **^{1}H-NMR** (500 MHz, DMSO-d_6): δ 0.93 (t, J = 6.8 Hz, 3H), 1.31 (broad, 2H), 1.56 (broad, 2H), 3.34 (broad, 2H), 4.12 (s, 2H), 7.33 (s, 1H), 7.47 (d, J = 8.1 Hz 2H), 7.82–7.63 (s, 1H), 7.92 (d, J = 8.1 Hz, 2H), 12.56 (s, 1H); **^{13}C-NMR** (126 MHz, DMSO-d_6): δ 13.36, 19.09, 22.94, 37.18, 57.43, 108.97, 127.26 (strong), 128.23, 128.65 (strong), 130.06, 132.20, 132.92, 147.61, 148.66, 157.70, 166.45, 170.00; $C_{17}H_{18}ClN_5OS_3$, Exact Mass: 439.99; Observed Mass (M): 440.

*2.3.4. 2-((5-(butylamino)-1,3,4-thiadiazol-2-yl)thio)-N-(4-(p-tolyl) thiazol-2-yl) acetamide **(4d)***

m.p. 240–242 °C, yield: 90 %, brown powder; FT IR: 619, 732, 814, 1041, 1384, 1502, 1616, 3476 cm^{-1}; Elemental analysis calc %: C, 51.53; H, 5.05; N, 16.69; O, 3.81; S, 22.92; **^{1}H-NMR** (500 MHz, DMSO-d_6): δ 0.93 (m, 3H), 1.31 (m, 2H), 1.56 (m, 2H), 2.33 (m, 2H), 2.51 (s, 3H), 4.10 (s, 2H), 7.24 (d, J = 6 Hz, 2H), 7.33 (s, 1H), 7.57 (s, 1H), 7.78 (d, J = 6 Hz, 2H), 12.52 (s, 1H); **^{13}C-NMR** (126 MHz, DMSO-d_6): δ 13.43, 19.14, 20.74, 23.01, 57.57, 107.51, 125.58 (strong), 129.28 (strong), 131.65, 137.20, 148.62, 149.11, 157.43, 166.57, 168.02, 170.26; $C_{18}H_{21}N_5OS_3$, Exact Mass: 419.09; Observed Mass (M): 420.

*2.3.5. 2-((5-(butylamino)-1,3,4-thiadiazol-2-yl)thio)-N-(4-(4-nitrophenyl)thiazol-2-yl) acetamide **(4e)***

m.p. 276–278 °C, yield: 86 %, brown powder; FT IR: 620, 736, 825, 1052, 1384, 1518, 1617, 3475 cm^{-1}; Elemental analysis calc %: C, 45.32; H, 4.03; N, 18.65; O, 10.65; S, 21.35; **^{1}H-NMR** (500 MHz, DMSO-d_6): δ 0.93 (t, J = 7.3 Hz, 3H), 1.31 (sextet, J = 7.3 Hz, 2H), 1.62–1.52 (m, 2H), 3.20–3.13 (m, 2H), 4.13 (s, 2H), 7.33 (s, 1H), 8.02 (s, 1H), 8.16 (d, J = 8.9 Hz, 2H), 8.31 (d, J = 8.9 Hz, 2H), 12.66 (s, 1H); **^{13}C-NMR** (126 MHz, DMSO-d_6): δ 13.68, 19.11, 22.96, 37.35, 57.44, 112.85, 124.30 (strong), 126.80 (strong), 140.06, 146.74, 148.70, 158.18, 166.74, 170.07; $C_{17}H_{18}N_6O_3S_3$, Exact Mass: 450.55; Observed Mass (M+1): 453.

*2.3.6. 2-((5-(butylamino)-1,3,4-thiadiazol-2-yl)thio)-N-(4-(4-fluorophenyl)thiazol-2-yl) acetamide **(4f)***

m.p. 218–222 °C, yield: 89 %, dark brown powder; FT IR: 620, 736, 825, 1052, 1384, 1518, 1617, 3475 cm^{-1}; Elemental analysis calc %: C, 48.21; H, 4.28; F, 4.49; N, 16.54; O, 3.78; S, 22.71; **^{1}H-NMR** (500 MHz, DMSO-d_6): δ 0.94 (t, J = 7.4 Hz, 3H), 1.40–1.24 (m, 2H), 1.69–1.46 (m, 2H), 2.51 (s, 2H), 3.17 (dd, J = 9.9, 7.0 Hz, 2H), 6.97 (s, 1H), 7.04 (s, 1H), 7.18 (t, J = 8.9 Hz, 2H), 7.82 (dd, J = 8.9, 5.6 Hz, 2H), 11.02 (s, 1H); **^{13}C-NMR** (126 MHz, DMSO-d_6): δ 13.35, 19.08, 22.94, 38.91, 57.41, 101.05, 115.18 (strong), 127.34 (strong), 129.60, 131.73, 135.01, 148.65, 160.42, 162.57, 168.15; $C_{17}H_{18}FN_5OS_3$, Exact Mass: 423.54; Observed Mass (M): 424.

*2.3.7. 2-((5-(butylamino)-1,3,4-thiadiazol-2-yl)thio)-N-(4-(3-nitrophenyl)thiazol-2-yl) acetamide **(4g)***

m.p. 238–240 °C, yield: 85 %, brown powder; FT IR: 621, 754, 1055, 1381, 1514, 1617, 3414 cm^{-1}; Elemental analysis calc %: C, 45.32; H, 4.03; N, 18.65; O, 10.65; S, 21.35; **^{1}H-NMR** (500 MHz, DMSO-d_6): δ 0.94 (t, J = 7.2 Hz, 3H), 1.32 (sextet, J = 7.0 Hz, 2H), 1.58 (broad, 2H), 3.15 (m, 2H), 4.14 (s, 2H), 7.35 (m, 1H), 7.74 (m, 1H), 7.98 (s, 1H), 8.18 (m, 1H), 8.35 (m, 1H), 8.73 (s, 1H), 12.67 (s, 1H); **^{13}C-NMR** (126 MHz, DMSO-d_6): δ 13.40, 19.13, 37.21, 57.48, 112.74, 124.17 (strong), 126.49 (strong), 140.06, 146.45, 146.74, 148.70, 158.18, 166.74, 170.07; $C_{17}H_{18}N_6O_3S_3$, Exact Mass: 450.55; Observed Mass (M+2): 454.

*2.3.8. N-(4-(3-bromophenyl)thiazol-2-yl)-2-((5-(butylamino)-1,3,4-thiadiazol-24yl)thio) acetamide **(4h)***

m.p. 190–192 °C, yield: 86 %, light brown powder; FT IR: 621, 754, 1055, 1381, 1514, 1617, 3414 cm^{-1}; Elemental analysis calc %: C, 42.15; H, 3.75; Br, 16.49; N, 14.46; O, 3.30; S, 19.85; **^{1}H-NMR** (500 MHz, DMSO-d_6): δ 0.93 (t, J = 7.3 Hz, 3H), 1.31 (sextet, J = 7.3 Hz, 2H), 1.56 (broad, 2H), 3.15 (t, J = 7.0 Hz 2H), 4.15 (s, 2H), 7.33 (t, J = 2.3 Hz 1H), 7.40 (t, J = 7.5 Hz, 1H), 7.52 (dt, J = 7.5 Hz & 2.3 Hz, 1H), 7.81 (s, 1H), 7.91 (dt, J = 7.5 Hz & 2.3 Hz, 1H), 8.10 (s, 1H), 12.57 (s, 1H); **^{13}C-NMR** (126 MHz, DMSO-d_6): δ 13.37, 19.10, 22.95, 37.18, 57.43, 109.73, 122.09, 124.44, 130.35, 128.18,130.86, 136.29, 147.10, 148.67, 157.72, 166.51, 170.02; $C_{17}H_{18}BrN_5OS_3$, Exact Mass: 484.98; Observed Mass (M + 2): 487.

*2.3.9. 2-((5-(butylamino)-1,3,4-thiadiazol-2-yl)thio)-N-(4-(3-methoxyphenyl)thiazol-2-yl)acetamide **(4i)***

m.p. 224–228 °C, yield: 89 %, brown powder; FT IR: 480, 621, 802, 1074, 1384, 1514, 1617, 3472 cm^{-1}; Elemental analysis calc %: C, 49.63; H, 4.86; N, 16.08; O, 7.35; S, 22.08; **^{1}H-NMR** (500 MHz, DMSO-d_6): δ 0.93 (s, 3H), 1.31 (s, 2H), 1.56 (s, 2H), 3.16 (s, 2H), 4.11 (s, 2H), 3.81 (s, 3H), 6.91 (m, 2H), 7.33 (s, 1H), 7.47 (m, 1H), 7.65 (m, 1H), 12.55 (s, 1H); **^{13}C-NMR** (126 MHz, DMSO-d_6): δ 13.36, 19.08, 22.94, 54.98, 57.43, 66.89, 108.61, 110.79, 111.13, 113.57, 117.93, 129.71, 135.43, 148.68, 157.41, 159.49, 166.41, 170.02; $C_{18}H_{21}N_5O_2S_3$, Exact Mass: 435.57; Observed Mass (M): 436.

*2.3.10. 2-((5-(butylamino)-1,3,4-thiadiazol-2-yl)thio)-N-(4-(2-oxo-2H-chromen-3-yl)thiazol-2-yl) acetamide **(4j)***

m.p. 216–220 °C, yield: 90 %, faint yellow powder; FT IR: 480, 621, 723, 849, 1059, 1382, 1506, 1617, 3473 cm^{-1}; Elemental analysis calc %: C, 50.72; H, 4.04; N, 14.79; O, 10.13; S, 20.31; **^{1}H-NMR** (126 MHz, DMSO-d_6): δ 0.92 (broad, 3H), 1.30 (broad, 2H), 1.56 (broad, 2H), 3.16 (broad, 2H), 4.13 (s, 2H), 7.75–7.01 (m, 3H), 7.84 (s, 1H), 8.09 (m, 2H), 8.58 (s, 1H), 12.59 (s, 1H); **^{13}C-NMR** (126 MHz, DMSO-d_6): δ 13.37, 19.10, 22.95, 37.24, 57.44, 114.40, 115.83, 118.90, 120.20, 124.66, 128.80, 131.84, 138.50, 142.07, 148.61, 152.35, 157.27, 158.64, 166.65, 170.05; $C_{20}H_{19}N_5O_3S_3$, Exact Mass: 474.06; Observed Mass (M): 475.

*2.3.11. Ethyl 2-(2-((5-(butylamino)-1,3,4-thiadiazol-2-yl)thio) acetamido)-4-methyl-thiazole-5-carboxylate **(4k)***

m.p. 218–220 °C, yield: 89 %, brown powder; FT IR: 1382, 1510, 1620, 3415 cm^{-1}; Elemental analysis calc. %: C, 43.36; H, 5.09; N, 16.85; O, 11.55; S, 23.15; **^{1}H-NMR** (500 MHz, DMSO-d_6): δ 0.94 (t, J = 7.3 Hz, 3H), 1.28 (t, J = 7.1 Hz, 3H), 1.57 (m, 2H), 1.80 (m, 1H), 2.56 (s,3H), 3.17 (t, J = 8 Hz, 2H), 4.10 (s, 2H), 4.25 (q, J = 7.1 Hz, 2H), 7.11 (s, 1H), 7.33 (s, 1H), 12.74 (s, 1H); **^{13}C-NMR** (126 MHz, DMSO-d_6): δ 13.36, 14.06, 16.88, 25.12, 22.89, 37.16, 60.45, 114.21, 136.40, 148.37, 156.13, 159.12, 161.89, 167.10, 170.06. $C_{15}H_{21}N_5O_3S_3$, Exact Mass: 415.08; Observed Mass (M): 415.3.

2.4. Antituberculosis activity studies

2.4.1. Disk diffusion assay

The antitubercular activities of the synthesized compounds were evaluated by the reported method [26]. Sterile Whatman paper disks were impregnated with the synthesized compounds (50 micro lit of concentration having 1 mg/mL). Standard used was Rifampicin (1 mg/mL). The respective disks were positioned on the sterile solidified Middlebrook 7H 10 agar medium and later spread with the culture of *M. tuberculosis* inoculums. The petri plates were diffused in refrigerator for 1 h and then shifted to the incubator at 37 °C for 5 days. The inhibition zones were measured by a zone measuring scale [27,28].

2.4.2. Resazurin microtiter plate assay

The REMA plate assay was carried out as described [27]. Briefly, 100 μL of 7H9–S (composing 0.5 % glycerol supplemented with oleic acid, dextrose, 0.1 % casitone, catalase, and albumin) broth was added in all the wells of a sterile flat-bottom 96-well plate, and then serial twofold dilutions were prepared directly in the plate of each screened compound. 100 μL of inoculums was added to each well. The plate was sealed with a sterile plastic bag and incubated at 37 °C for 7 days. 30 μL of (0.01 % in sterile d/w) resazurin solution was added to each well, and the plate was reintubated for additional one day. A color change from blue to pink indicates the growth of organisms. MIC was the lowest concentration of the drug, which prevented color change. The drugs concentration was in the range 0.097–50 μg/mL and for RIF, 0.097–50 μg/mL.

2.4.3. Hydroxyl radical assay

The Fenton reaction demonstrated the (OH) radical activity. The reaction mixture of 90 μL of 1–10 phenanthroline (1 mM), 60 μL of $FeCl_3$ (1 mM) and 150 μL of H_2O_2 (0.17 M), 2.4 mL of phosphate buffer (0.2 M, pH 7.8) and 1.5 mL of individual synthesized compound (1 mg/mL) were mixed. The reaction was initiated by adding hydrogen peroxide. After 5 min of incubation at room temperature, the absorbance was measured at 560 nm. Ascorbic acid (1 mM) was used as a reference standard.

% radical scavenging activity $= 1 - (T \div C)100$ where T is the absorbance of test sample and C is the absorbance of control sample.

2.4.4. 2, 2-diphenyl-1-picrylhydrazyl radical scavenging assay (DPPH)

The electron transfer capabilities of the synthesized compounds were measured by the bleaching of the purple-colored methanolic solution of DPPH. Equal volume of the compound and DPPH solution in methanol were mixed so that the final volume of reached 3 mL. Next, incubated the samples for 20 min at R.T. and measured the absorbance at 517 nm. 1 mM ascorbic acid was used as a standard. The inhibition percentage was calculated using the following formula [28], radical scavenging activity $= 1 - (T \div C)100$ where, T is the absorbance of test sample and C is the absorbance of control sample.

2.4.5. Hemolytic activity

The hemolytic activities using human RBCs for the selected screened compounds were determined following the literature method [29]. Human blood (5 mL) was initially collected in tubes containing 1 mg of EDTA (anti-coagulant). The erythrocytes were collected by centrifugation at 2000 rpm at 20 °C for 10 min. The collected pellet was washed thrice with PBS. Then, 10 % (v/v) erythrocytes/PBS suspension was prepared using Phosphate buffered saline (PBS). From this, 1:10 dilution was prepared using PBS, which was used for the assay. 100 μL of erythrocytes were added to each well containing synthesized compounds 100 μL (500 μg/mL). 0.001 N Triton X 100 was used as a reference compound. The tubes were incubated for 1 h at 37 °C and centrifuged repeatedly. From the supernatant, 150 μL solution was transferred to 96 well microplates, and the absorbance was measured at 540 nm using a plate reader. hemolysis was calculated using the following equation,

Hemolysis = [(Absorbance at 540 nm of sample - Absorbance at 540 nm of buffered sample) ÷ (Absorbance at 540 nm of Triton X -100 treated sample - Absorbance at 540 nm of buffered sample)] ×100

Statistical analysis: All the biological experiments were conducted intriplicate and the results are shown to be the mean values of three independent experiments. Antioxidants activities were shown to be n = 3, ±SD.

2.5. In-silico study

2.5.1. Target prediction

Target prediction was carried out using PharmMapper Webserver [30]. The three-dimensional structure of compound **4b** was provided as an input for the prediction because of its MIC value relative to the other compounds. The target was manually selected from a library depending upon the scoring results provided by PharmMapper.

2.5.2. Molecular docking studies

This study utilizes an established molecular docking protocol [31–36]. The details relevant to this study are described below.

2.5.3. Target preparation

The three-dimensional structure of the predicted target was obtained from the Protein Data Bank (https://www.rcsb.org/). The structure corresponds to PDB ID: 2QC3 which is a structure of the malonyl coenzyme A (CoA)-acyl carrier protein (ACP) trans acylase (MCAT) solved by X-ray diffraction at 2.3 Å [37]. The active site of MCAT in its crystallized state consists of an acetate molecule which is considered as a substrate mimic of malonate. The acetate molecule was excluded prior to docking. The "Make macromolecule" command implemented in PyRX v0.8 was used to convert the protein molecule in the "pdbqt" format and charges were assigned to its coordinates.

2.5.4. Ligand preparation

The ligands were constructed manually in their two-dimensional states using Marvin Sketch 23.3 (http://www.chemaxon.com). Next, they were converted to their respective three-dimensional conformations by using the "clean in 3D" command ant then saved in "sdf" format. The ligands were then manually compiled in a single file to create a library. The library was imported into PyRx and the compounds were minimized using the UFF force field and conjugate gradient optimization algorithm. The ligands were converted to "pdbqt" format prior to docking.

2.5.5. System validation and molecular docking

Molecular docking was carried out using Auto Dock 4.2.6 implemented in PyRx [38]. The docking system was validated using the acetate molecule originally present in the crystal structure. The acetate molecule was removed and redocked inside the active site of MCAT and the quality of docking was evaluated using the Root Mean Square Deviation (RMSD) of the docked and crystallographic pose with respect to heavy atoms. A deviation of 2 Å between the crystallographic and the docked pose is acceptable as per the literature [39]. In this case, the deviation was 0.35 Å which confirms the suitability of the docking system. Autogrid4 was used to create a grid around the active site. The grid box of dimensions 60 × 60 × 60 Å with grid spacing 0.375 Å was placed to cover the active site residues (Gln9, Ser91, Val92, Arg116, Phe193, His194) and the active site cavity.

Lamarckian genetic algorithm was used to generate ten poses of each docked ligand. The algorithm parameters were set to 10 runs of each genetic algorithm (GA), number of individuals in population was set to 150, maximum number of generations were set to 27000, the rate of mutation was set to 0.02 and the rate of crossover was set to 0.8 while all

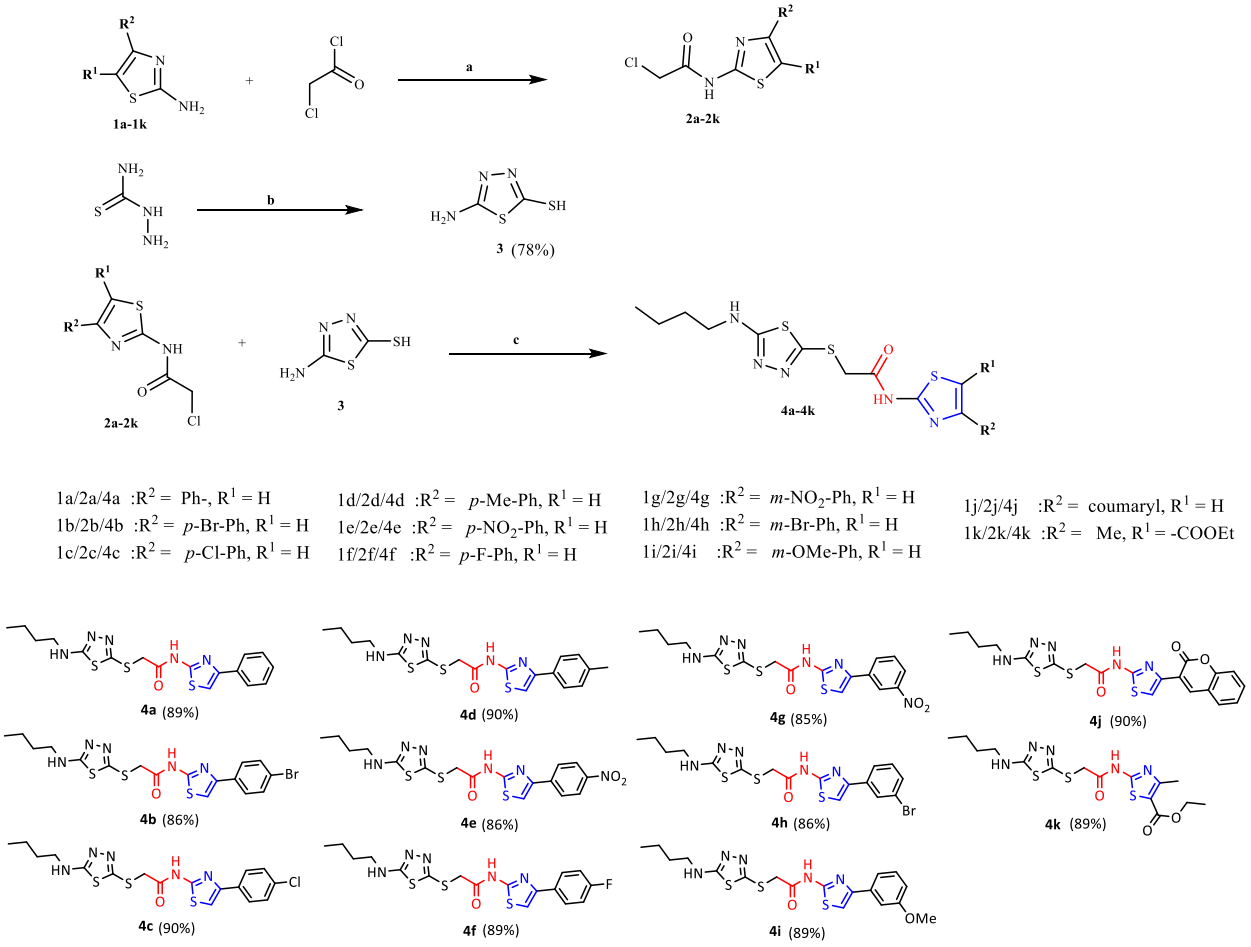

Scheme 1. General synthetic routes to access the novel thiadiazol-thiazole derivatives (**4a-4k**).

other parameters were kept as default. The best ranked poses for each compound (one with the lowest binding energy) were used to generate the docking images.

2.5.6. ADMET study

ADMET (absorption, distribution, metabolism, and excretion) studies were carried out for the best scoring compounds in molecular docking studies (**4b, 4d, 4f** and **4k**) using Swiss ADME webserver [40]. The webserver is one of the premier platforms for the predictions of ADME properties of chemical compounds. It utilizes computational models based upon comprehensive datasets and rigorous validation which can offer reliable predictions of physiochemical, pharmacokinetic and pharmacodynamic properties, drug-likeness, medicinal chemistry friendliness of the compounds. These properties are crucial for the assessment of a compound to be a potential drug candidate. These initial understandings can greatly facilitate the drug development process by identifying suitable candidates for subsequent experimental evaluation.

2.5.7. Toxicity study

In silico methods have showcased their ability in predicting the safety profiles of chemical compounds [41]. Following the same, toxicity analysis was carried out for the best scoring compounds (**4b, 4d, 4f** and **4k**) based on results from molecular docking studies using ProTox 3.0 webserver [42]. ProTox 3.0 utilizes molecular similarity and machine learning based approaches to predict toxicity endpoints for the input compounds. These include organ toxicity, clinical toxicity, acute toxicity, adverse outcome pathways, molecular initiating events along with several other endpoints.

The compounds were provided to the webserver in SMILES format. Toxicity predictions were carried out for all available end points by selecting the "All'' option. These include toxicity estimators such as hepatotoxicity, neurotoxicity, nephrotoxicity, cardiotoxicity, respiratory toxicity, carcinogenicity, immunotoxicity, cytotoxicity, mutagenicity, BBB-barrier, clinical toxicity and nutritional toxicity. Additionally, the interactions of the compounds with receptors of the nuclear signaling pathways such as Aryl hydrocarbon Receptor (AhR), Androgen Receptor (AR), Estrogen Receptor Alpha (ER), Estrogen Receptor Ligand Binding Domain (ER-LBD), along with others, were examined. Moreover, interactions with the proteins of the stress response pathway, molecular initiating events and cytochrome metabolism were also examined.

3. Results and discussion

During the synthesis of novel 2-((5-(butylamino)-1,3,4-thiadiazol-2-yl)thio)-N-(thiazol- 2-yl) acetamide derivatives (**4a-4k**), TBAB played dual role as a catalyst and butylating agent for the synthesis of eleven thiazole-1,3,4-thiadiazole acetamide derivatives (**4a-4k**) (Scheme-1). We proposed that TBAB is present in an intimate ion pair with KI in ether at room temperature.

Reaction conditions: a. TEA (1.3 equiv.), DMF, 0–5 °C, reaction time 1–4 h; **b.** anhydrous Na_2CO_3 (1 equiv.), CS_2 (1 equiv.), absolute ethanol, reaction time 10 h; **c.** TBAB (1.0 equiv.), K_2CO_3 (1 equiv.), KI (0.025 equiv.), THF, reaction time: 20–24 h.

3.1. Synthetic chemistry

Optimization studies involving synthesis of **4e from** 2-chloro-N-(4-

Table 1
Optimization of base and solvent for synthesis of **4e**.

Entry	Base	Yield (%) 4e[a]		
		THF	1,4 Dioxane	Methyl-butyl Ether
1	DBU	48	[b]NR	51.2
2	Piperidine	[b]NR	25.5	55.0
3	Triethyl amine	[b]NR	[b]NR	[b]NR
4	Potassium carbonate	82	42	60
5	Cesium carbonate	78	44	51.2
6	Sodium acetate	56	44	60.1

Reaction conditions: 2e (1.0 equiv.), **3** (1.0 equiv.), TBAB (1.0 equiv.), Base (1 equiv.), KI (0.025 equiv.), Solvent (20 vol with respect to the reactant **2e**).
[a] Isolated % yield.
[b] NR: No reaction.

Table 2
Optimization of equivalent mole ratio of TBAB, K_2CO_3 in THF.

Entry	TBAB	K_2CO_3	Volume of THF (in mL) with respective to TBAB	Time (hrs.)	Yield (%) 4e[a]
1	1.0	0.5	30	62	33
2	1.0	0.7	30	61	45
3	1.0	1.0	30	58	56
4	1.1	1.0	30	56	67
5	1.2	1.0	30	56	74
6	**1.1**	**1.1**	**30**	**48**	**90**
7	1.1	1.2	30	48	81
8	1.2	1.3	30	48	77
9	1.1	1.1	20	45	82
10	1.1	1.1	20	48	85

Reaction conditions: 2e (1.0 equiv.), 3 (1.0 equiv.), KI (0.025 equiv.), THF.
[a] Isolated yield.

(4-nitrophenyl) thiazol-2-yl) acetamide (**2e**) was clubbed with 5-amino-1,3,4-thiadiazole-2-thiol (**3**). Simultaneously butylation of the amino group by using TBAB, KI with three different solvents either THF/1,4-dioxane/methyl-butyl ether by using organic or inorganic bases at room temperature. (Table 1).

Reactions involving inorganic bases such as potassium carbonate, cesium carbonate, and sodium acetate, were carried out in three different solvents namely tetrahydrofuran, 1,4-dioxane and methyl *t*-butyl ether (Table 1, entries 4–6), while with the organic base triethylamine, the reaction did not proceed (Table 1, entries 3). However, when 1,8-Diazabicyclo [5.4. 0]undec-7-ene (DBU) and piperidine were screened, the reaction afforded less yield (Table 1, entries 1–2). Interestingly, using cesium carbonate, the reaction afforded **4e** in acceptable yields of 44–78 % (Table 1, entries 5), while another base, sodium acetate, afforded the corresponding compound **4e** in 44–60 % yield (Table 1, entry 6). These encouraging results suggested that potassium carbonate to be the most suitable base in THF to synthesize **4e** (Table 1, entry 4). Optimization experiment for mole ratio of TBAB, K_2CO_3 in THF with respective **2e** (1.0 equiv.), concluded that reaction is more favorable in the ratio 1:1.1:1.1(**2e**: TBAB: K_2CO_3) in 30 volume of solvent. (Table 2, entry 6).

The optimized reaction conditions for synthesis of **4e**, were then employed for the synthesis of novel compounds (**4a-4k**) starting from 2-aminothiazoles derivatives (**1a-1k**) (Scheme-1). 2-aminothiazoles derivatives (**1a-1k**) on reaction with chloro acetyl chloride (CAC) furnished N-thiazol-2-yl-2-chloroacetamide derivatives (**2a-2k**) in excellent yields. The compound **3** was synthesized by condensation of thiosemicarbazide with carbon disulfide using sodium carbonate as a base. The optimized method for synthesis of (**4a-4k**) worked equally well for mono, di, tri-substituted thiadiazol-thiazole derivatives with excellent yields. Also, it was observed that R^2 having electron-donating groups *p*-Br, *m*-Br, *p*-Cl, *p*-Me, *p*-F, and electron-withdrawing groups such as *m*-Br, *m*-OMe, *p*-NO_2, *m*-NO_2, -COOEt were well tolerated to afford synthesized compounds (**4a-4k**) in excellent yields.

3.2. Role of TBAB

TBAB is a promising non-metallic homogeneous phase-transfer catalyst [43]. In addition to its remarkable chemical stability, it is a non-corrosive, inexpensive, and readily available ammonium salt [44]. The NH groups of aromatic amines [45], amides [46], lactams [47], sulfonamides [48], and other heterocyclic nitrogen-containing compounds have all been effectively alkylated [49]. In 2021, Ekta Verma and co-workers reported the N-alkylation of anhydride and isatin derivatives [50]. In 2022, Ricardo Acosta Ortiz and co-workers reported the synthesis of a curing agent derived from limonene. They are used for the alkylation of primary amino groups with allyl bromide, TBAB, and sodium hydroxide [51]. However, reports for the alkylation of compound **3** are still limited.

Herein, we propose that a mixture of TBAB and KI remain as an intimate ion pair in ether solvent (Fig. 3). This intimate ion pair can be largely exploited for butylation of various compounds. The iodide species plays a dual role as a nucleophile and as a leaving group in the generation of butyl cation source. Out of the two nucleophilic centres, thiol (-SH) and amino (-NH_2) group of compounds **3**, initially the strong

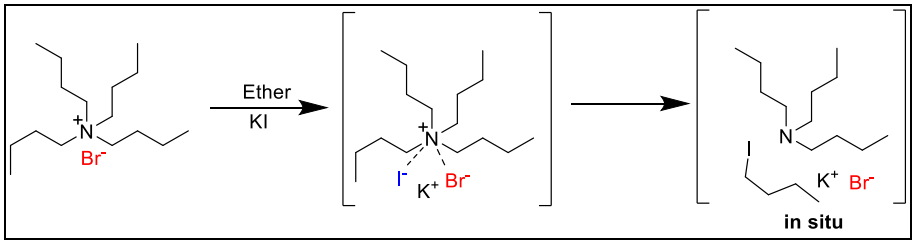

Fig. 3. Formation of intimate ion pair between TBAB and KI with subsequent *in situ* generation of n-butyl iodide.

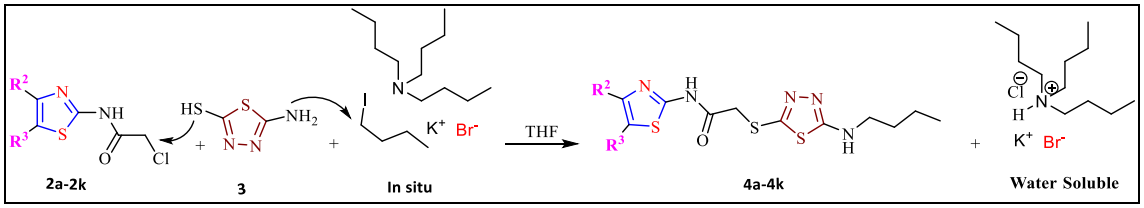

Fig. 4. Mechanism for synthesis of compounds (**4a-4k**).

Table 3
DEPT spectral analysis of **4e**.

Types of Carbon of compound 4e	DEPT subspectrum and chemical shift (in ppm)			
	DEPT-135	Deviation	DEPT-90	Deviation
$-CH_3$	13.68	Positive	13.68	NO
$-CH_2-$	19.11	Negative	19.11	NO
$-CH_2-$	22.96	Negative	22.96	NO
$-CH_2-$	37.35	Negative	37.35	NO
$-CH_2-$	57.44	Negative	57.44	NO
	112.85	Positive	112.85	Positive
	124.3 (strong)	Positive	124.3 (strong)	Positive
	126.80 (strong)	Positive	126.80 (strong)	Positive
	140.06	NO	140.06	NO
	146.74	NO	146.74	NO
	148.70	NO	148.70	NO
	158.18	NO	158.18	NO
	166.74	NO	166.74	NO
	170.07	NO	170.07	NO

NO: Not observed peak.; Positive deviation in DEPT-135 subspectrum: peak of either methine (-CH<) or methyl ($-CH_3$) group.; Negative deviation in DEPT-135 subspectrum: peak of methylene ($-CH_2-$) groups.; Positive deviation in DEPT-90 subspectrum: peak of methine (-CH<).; Peak not observed in DEPT 135 subspectrum and DEPT 90 subspectrum: quaternary carbon.

nucleophile thiol attacks on the carbon bearing chlorine (Cl–CH_2–C═O) of N-thiazol-2-yl-2-chloroacetamide derivatives (**2a-2k**) and next the amino group of compounds **3** attacks on the butyl carbon bearing iodine. The reaction offers moderate to excellent yields of the target compounds **4a-4k** (Fig. 4).

3.3. Spectral analysis

The structures of the synthesized compounds were well characterized by different spectroscopic techniques such as FT IR, ^{1}H-NMR, ^{13}C-NMR and MS. The compound **4e** is also characterized by DEPT (Table 3) and 2D techniques as COSY, HETCOR and HMBC. The FT IR spectra of the compounds (**4a-4k**) display characteristic four bands, the first band at ~3400 cm^{-1} assigned to νN–H, the second band at 610-690 cm^{-1} indicates νC-S, the third band at ~2000 cm^{-1} is assigned to νS-C═N whereas fourth band at 1620-1640 cm^{-1} is ascribed to νC═O of amide linkage. The one located at 1500–1300 cm^{-1} is due to the stretching band of νC═N and νC═C confirming the presence of imine and aromatic skeleton. The ^{1}H-NMR spectra of all compounds show clear and recognizable singlet peak for NH proton at ~ 12.5 ppm. The thiazole ring proton and methylene group protons of -S–CH_2–CO-N- is observed as a singlet for all compounds (**4a-4k**). The one methyl group (~0.9 ppm), three methylene groups (~1.0–4.5 ppm) present in butyl group showed multiplet having coupling constant 7–9 Hz or showed broad peak in ^{1}H-NMR spectra of compounds (**4a-4k**). The aromatic protons signal

Table 4
Minimum inhibitory concentration (MIC) of **4a-4k** and **3** against *M. tuberculosis* H37Ra.

Compound	Zone of inhibition	MIC (in μg/mL)
4a	+	208.33 ± 72.17
4b	+++	**7.81 ± 0**
4c	++	52.08 ± 18.04
4d	+	208.33 ± 72.17
4e	++	125 ± 0
4f	++	52.08 ± 18.04
4g	+	208.33 ± 72.17
4h	NZ	500 ± 0
4i	+	250 ± 0
4j	NZ	52.08 ± 18.04
4k	++	52.08 ± 18.04
3	+++	3.90 ± 0
Rifampicin	+++	2.60 ± 1.13

+= < 5 mm, ++= >5 & <10 mm, +++= >10 & < 18 mm, NZ=No zone, NA= Not applicable, n = 3, ±SD = 3.

Table 5
IC_{50} values of antioxidant activities of synthesized compounds **4a-4k** and **3**.

Compound	DPPH (mg/mL)	OH (mg/mL)
4a	32.25 ± 0.72	29.32 ± 0.1
4b	**33.76 ± 0.32**	**29.56 ± 0.35**
4c	29.33 ± 0.25	34.6 ± 0.2
4d	46.33 ± 0.11	32.6 ± 0.2
4e	26.73 ± 0.23	29.26 ± 0.25
4f	38.4 ± 0.34	33 ± 0.17
4g	35.5 ± 0.36	35.46 ± 0.30
4h	31.93 ± 0.47	31.96 ± 0.20
4i	43.63 ± 0.05	43.73 ± 0.23
4j	37.63 ± 0.83	35.6 ± 0.26
4k	34.66 ± 0.23	28.93 ± 0.61
3	43.46 ± 0.30	45.74 ± 0.05
Ascorbic acid	49.56 ± 0.20	NA
α-Tocopherol	NA	49.86 ± 0.66

NA= Not applicable, n = 3 ± = SD.

Table 6
Cytotoxicity data for compounds **4a-4k** and **3** against RBCs.

Compound	% Cytotoxicity
4a	0.84
4b	**0.45**
4c	1.3
4d	1.04
4e	0.15
4f	0.87
4g	0.76
4h	0.67
4i	0.78
4j	0.68
4k	1.03
3	**0.68**
Triton X-100	11.3

The synthesized compounds **4a-4k** and **3** exhibit very low to negligible cytotoxicity towards RBCs.

Table 7
Docking results.

Compound	Binding energy (kcal/mol)
4a	−6.41
4b	**−7.54**
4c	−6.36
4d	**−7.01**
4e	−6.29
4f	**−7.25**
4g	−5.57
4h	−6.11
4i	−6.82
4j	−6.24
4k	**−7.14**

observed in between 6.5 and 8.5 ppm and they showed either ortho coupling (J = ~ 8 Hz) or *meta* coupling (J = ~ 2 Hz). The ^{13}C-NMR of all compounds displayed all the signals at the expected chemical shift values. There are five aliphatic SP^3 hybridised carbon signals in all compounds (**4a-4k**) from 13 to 60 ppm. The important peak in all compounds (**4a-4k**) is at ~ 170 ppm which is a characteristic peak of amidic carbonyl carbon (O═C–N). The MS spectra of all compounds exhibit either molecular ion peak (M^+) or isotopic peaks. In DEPT-135 subspectrum of compound **4e**, 13.68 ppm appear in positive deviation but not observed in DEPT-90 subspectrum indicate that it is $–CH_3$ group. The DEPT-135 subspectrum of compound **4e** exhibited four peak of aliphatic methylene group (19.11 ppm, 22.96 ppm, 37.35 ppm and 57.44 ppm) in negative deviation but not observed in DEPT-90 subspectrum whereas one peak of methyl (at 13.68 ppm) in positive deviation in DEPT-135 subspectrum. The expected three type of aromatic carbons -CH= (112.85 ppm, 124.3 ppm (strong), 126.80 ppm (strong) observed in DEPT-135 and DEPT-90 subspectrum in positive deviation.

As expected, peaks for six quaternary carbons (140.06 ppm, 146.74 ppm, 148.70 ppm, 158.18 ppm, 166.74 ppm, 170.07 ppm) do not observed in DEPT-135 and DEPT-90 subspectrum, but relevant peaks appear in HMBC spectra through two and three bond coupling between C–H. From HETCOR and HMBC it is confirmed that the peak of quaternary carbons of 1,3,4 thiadiazole ring at 166.74 ppm and 170.07 ppm. HETCOR spectra also confirmed the expected coupling between C–H at ~0.9 ppm with 15 ppm, ~1.3 ppm with 21 ppm, ~1.6 ppm with 26 ppm, ~4 ppm with 39 ppm, ~3 ppm with 59 ppm, ~8.0 ppm with 115 ppm, ~8.2 ppm with 128 ppm, ~8.3 ppm with 126 ppm. The COSY spectra give the one bond homonuclear coupling between H–H at ~0.9 ppm with 1.3 ppm, ~1.3 ppm with 1.6 ppm, ~1.6 ppm with 3.2 ppm confirmed the butyl linkage, and ~8.36 ppm with 8.21 ppm confirmed *para* nitro aromatic di-substituted ring in **4e.**

3.4. Biological activities

3.4.1. Antitubercular activities

The antituberculosis assays were performed by disc diffusion method and results are summarized in Table 4. The novel 2-(5-(butylamino)-1,3,4-thiadiazol-2-ylthio)-N-(thiazol-2-yl) acetamide derivatives (**4a-4k**) were screened for antituberculosis activity against *M. tuberculosis* (H37Ra) and MIC values were determined by using Rifampicin as the standard.

The MIC values of synthesized compounds were assessed. Compounds **4b** and **3** showed the best MIC value 7.8125 μg/mL and 3.40 μg/mL, respectively. Compounds **4c, 4j, 4e,** and **4k** also exhibited moderate to good MIC activity towards microorganisms compared to the standards Rifampicin used. The results are expressed as the mean values of three independent experiments.

3.4.2. 2, 2-diphenyl-1-picrylhydrazyl (DPPH) and hydroxyl radical (OH) radical scavenging activity

2,2-diphenyl-1-picrylhydrazyl radical scavenging assay for (DPPH) and Hydroxyl radical (OH) were calculated (Table 4). The screened compounds exhibited moderate to good IC_{50} value of DPPH and OH radical scavenging activities compared to standard ascorbic acid and α-Tocopherol, respectively. It was observed that **4a, 4b, 4d, 4f,4g, 4i-4k** and **3** derivatives (1 mg/mL) were found to be potent DPPH reducing agents. The novel derivatives **4a-4k** and **3** are found to be promising OH radical scavengers as compared to α-Tocopherol. The results are summarized as the mean values n = 3 experiments standard deviation (SD).

3.4.3. Cytotoxicity studies

In-vitro haemolytic assays determined the haemolytic capability of the compounds against the host RBCs. The cytotoxicity of the synthesized compounds (**4a-4k**) towards RBCs was calculated by MTT assay. All the compounds (**4a-4k**) exhibited haemolytic activity below the threshold of 5 %, with most exhibiting activity below 0.1 % compared to the positive control Triton X-100 (11.3 %). The results revealed that all the screened compounds exhibit negligible cytotoxicity as compared to positive control Triton X-100 (Table 6).

3.4.4. Structure activity relationship

The thiadiazole-linked thiazole derivatives (**4a-4k**) exhibit a broad spectrum of anti-tubercular activities. Compound **4b**, containing *para* bromo substituted phenyl at R^2, is found to be more active as an anti-tubercular agent than other compounds containing coumaryl and aromatic substitutes. The synthesized compounds containing weak electron-donating substituents (**4c** and **4f**) exhibit more anti-tubercular activity than those containing moderate to strong electron-donating and strong electron withdrawing substituents like CH_3 (**4d**), and $–NO_2$ (**4e**) at *para* position. In *meta*-substituted compounds, a strong electron-withdrawing group such as $–NO_2$ (**4g**), -Br (**4h**) and -OMe (**4i**) shows less anti-tubercular activity than *para* substituents like -Br (**4b**) and $–NO_2$ (**4g**). The presence of a coumarin ring (**4j**) and aliphatic substituted compound (**4k**) have been found to exhibit potent anti-tubercular activity. The study suggests that moderate electron-donating substituents results in enhanced anti-tubercular activities. It has been accounted that weak electron-donating substituents increases the electron density, making the compounds efficient anti-tubercular agents and augmenting their anti-tubercular activity. Among halogens, the DPPH scavenging activity increases from chloro to bromo to fluoro substituents. Interestingly, it is observed that the OH radical scavenging activity increases from bromo to fluoro to chloro substituents. The radical scavenging study demonstrated that **4a-4k** exhibit promising antioxidant characteristics, as evidenced by their inhibitory effect on DPPH and OH radicals (Table 5). All the synthesized compounds **4a-4k** show strong antioxidant activity, implying that all compounds may minimize DPPH and OH radicals. All the synthesized compounds **4a-4k** showed negligible cytotoxicity, indicate that all compounds are less toxic effect.

3.5. In-silico study

3.5.1. Target identification

The PharmMapper webserver utilizes a pharmacophore-based search strategy for target identification [30]. A pharmacophore represents a set of functional groups essential for the recognition of the ligand by a receptor macromolecule. The server houses a pharmacophore repository (PharmTargetDB) which contains over 7000 receptor-based pharmacophore models. The server investigates the compatibility of the ligand and the target based upon common pharmacophore features and designates a “fit score”, which is a direct measure of the affinity between the ligand and target. With the help of the target search feature provided by PharmMapper and molecular docking studies, malonyl coenzyme A (CoA)-acyl carrier protein (ACP) trans acylase (MCAT) was identified as a potential target for the compounds **4a-4k.** A pharmacophore search using compound **4b** yielded a fit score of 4.65 and a total of 9 features were found to be common between the ligand and the target.

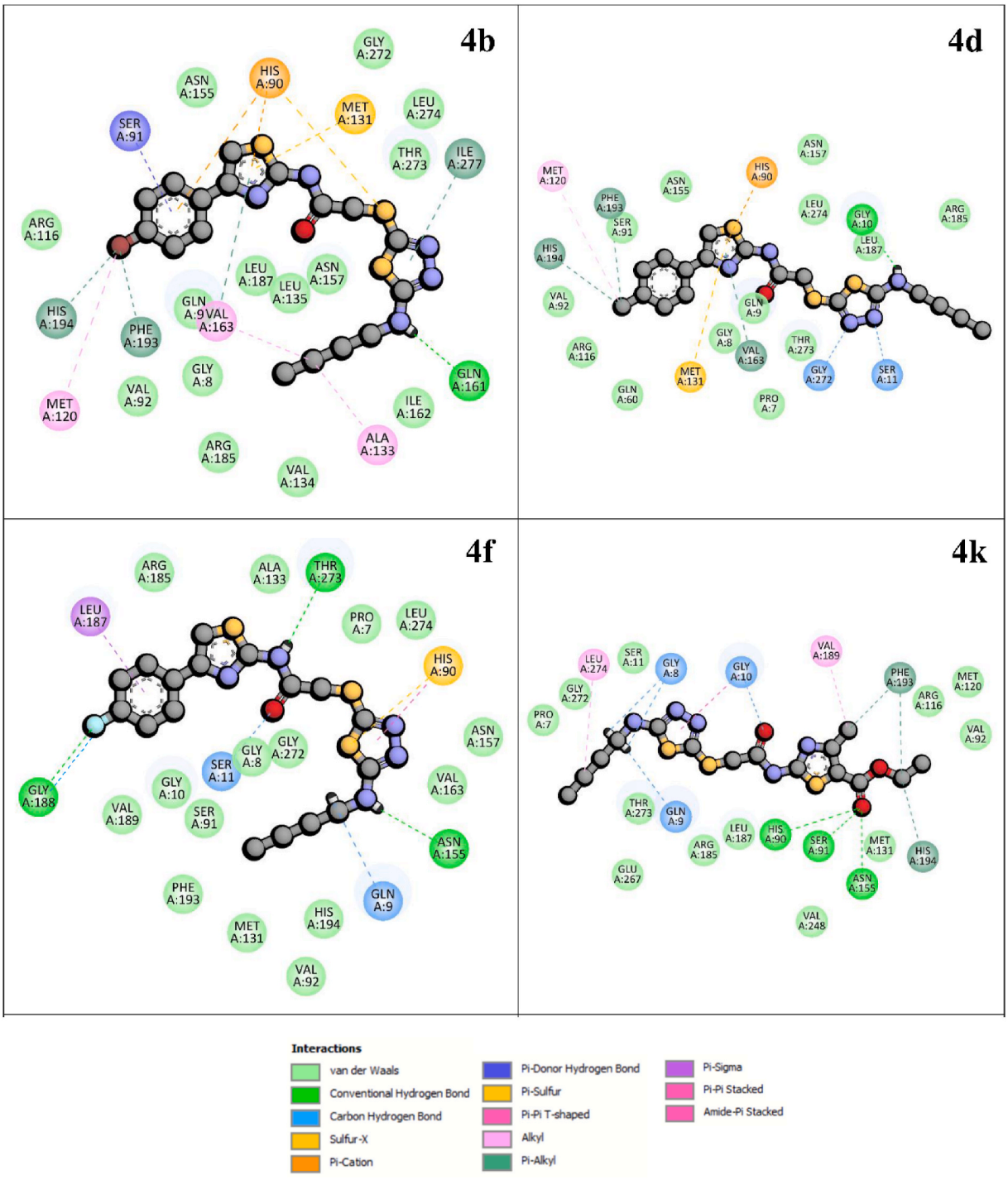

Fig. 5. 2D representation of the best scoring compounds **4b, 4d, 4f, 4k** in molecular docking studies along with interaction legend.

MCAT plays a crucial role in cell wall biosynthesis in *Mycobacterium tuberculosis* [52]. The main function of the enzyme is to transfer malonate from malonyl-CoA to the terminal thiol of holo-acyl carrier protein (ACP). The result of this transacylation reaction results in the formation of Malonyl ACP which acts as a substrate for fatty acid biosynthesis. Fatty acid biosynthesis enables *Mycobacterium tuberculosis* to survive in hostile environments. This makes MCAT a viable drug target for the design of anti-tuberculosis drugs.

3.5.2. *Docking results and interaction analysis*

The docking results indicate that all compounds (**4a-4k**) have affinity to the active site of MCAT. Considering that all these compounds show inhibitory potential in experiments, the docking results are in congruence. As per the UniProtKB reviewed (Swiss-Prot) entry of MCAT (UniProt ID: P9WNG5), MCAT has been annotated as a high-confidence drug target. The same entry also mentions that Ser91 and His194 are the active site amino acids with references to a manual homology-based inference. It can be observed from the docking results (Table 7 and Figs. 5–7) that these amino acids are involved in interactions with the ligands on numerous instances. Moreover, His90, which is situated directly next to Ser91 in the active site cavity, is involved in a plethora of interactions with all the compounds (**4a-4k**). This clearly points towards the plausible active site modulating ability of the compounds which could possibly hamper the binding of the natural substrate malonyl-CoA.

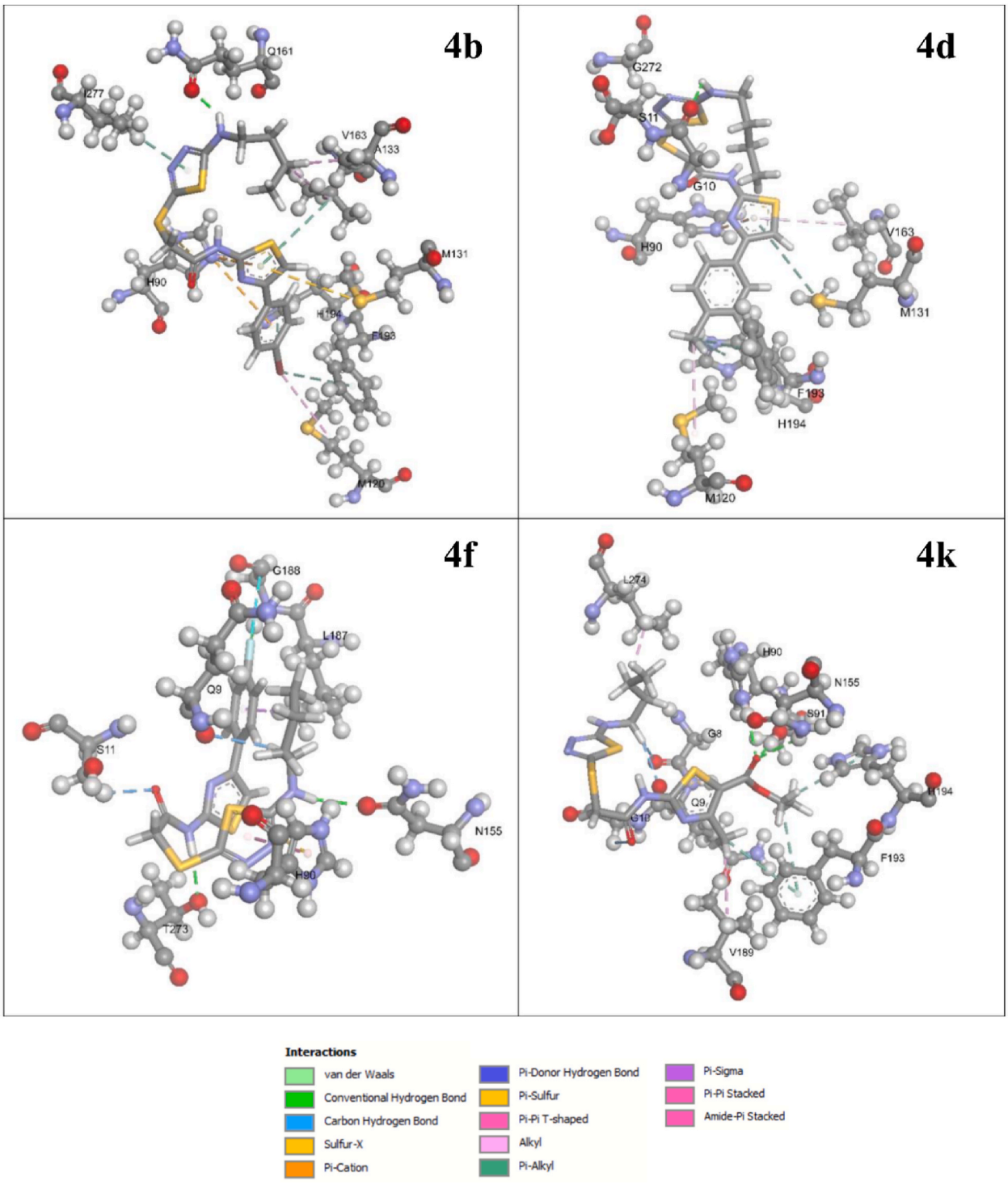

Fig. 6. 3D representation of the best scoring compounds **4b, 4d, 4f, 4k** in molecular docking studies along with interaction legend.

The compound **4b** has the best MIC value among the compounds (**4a-4k**) which is also validated by the docking results. This suggests that MCAT might be the most probable protein target of these compounds.

Alkyl and Pi-alkyl interactions appear to be crucial in stabilization of the protein-ligand complex in case of compound **4b**. Met120, Phe193, His194 form a hydrophobic pocket which allows the bromine atom of compound **4b** to bind to these amino acids simultaneously via alkyl and pi-alkyl interactions. The docking results suggest that the presence of either a halogen or carbon atom at this particular position in the ligand plays a crucial role for the nature of binding observed. Such mode of binding can also be seen in the case of compounds **4c** and **4d**. Ser91 is involved in a pi-donor hydrogen bond interaction with the aromatic ring of the bromobenzene moiety while Met131 interacts with the thiazole moiety through pi-sulfur interaction. His90 is also an important amino acid for the binding observed as it is involved in pi-cation interactions with bromobenzene and thiazole moieties as well as pi-sulfur interaction with the sulfur atom adjacent to the thiadiazole moiety. Ile277 stabilizes the thiadiazole moiety of compound **4b** via pi-alkyl interactions. Val163 interacts with the thiazole moiety through pi-alkyl interaction and along with Ala133, it forms alkyl interactions with one of the terminal carbon

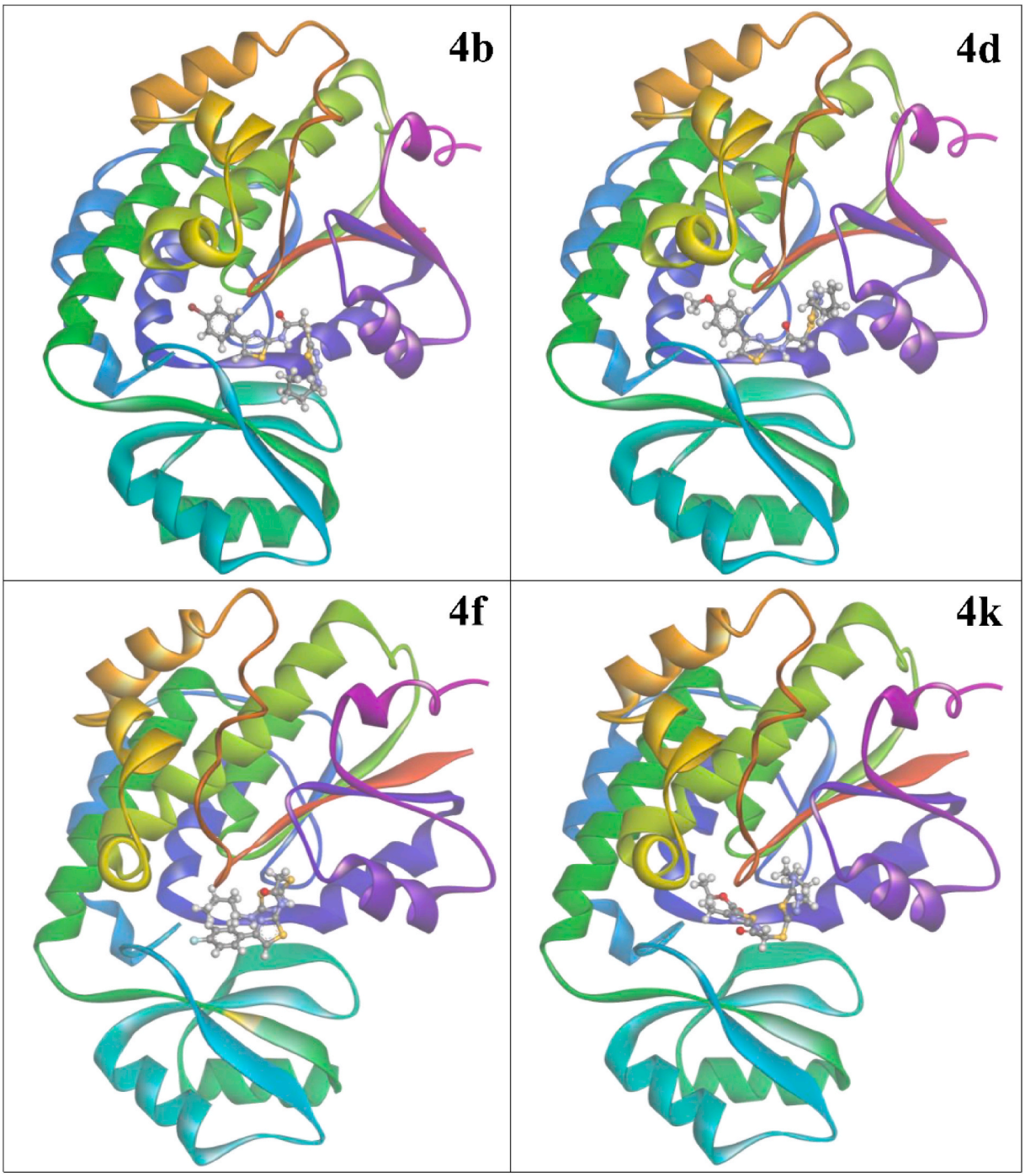

Fig. 7. 3D representation of the molecular docking results for the best scoring compounds **4b, 4d, 4f, 4k.**

atoms of the compound **4b**. The side chain oxygen atom from Gln161 acts as a hydrogen bond acceptor for the nitrogen atom adjacent to the thiadiazole moiety. Hydrogen bonds are known to play an important role in stabilization of protein-ligand complexes (Wade and Goodford, 1989).

In case of compound **4d**, many interactions could be seen in common when compared to the docking of compound **4b**, notably, the interactions of amino acids Phe193 and His194 with the non-aromatic carbon atom of the toluene moiety and the interactions of Met131, Val163, His90 with the thiazole moiety. However, the main chain oxygen atom from Gly9 acts as a hydrogen bond acceptor for the nitrogen atom adjacent to the thiadiazole moiety. The hydrogen atoms bound to the nitrogen atoms from the thiadiazole moiety appear to be interacting with the amino acids Gly272 and Ser11 through carbon-hydrogen bonds.

Compounds **4f** on the other hand differs significantly in its binding mode from compounds **4b** and **4d**. The fluorine atom from the fluorobenzene moiety is involved in a halogen bond with alpha carbon atom of Gly188. The nitrogen atom of Gly188 is also involved in a hydrogen bond with the fluorine atom. Leu187 forms a pi-sigma interaction to stabilize the fluorobenzene moiety. The side chain oxygen atom from Thr273 acts as a hydrogen bond acceptor for the nitrogen atom adjacent to the thiazole moiety. Ser11 interacts with the oxygen atom of the compound **4f** by a carbon-hydrogen bond. The side chain oxygen atom from Asn155 acts as a hydrogen bond acceptor for the nitrogen atom situated next to the thiadiazole moiety. The main chain oxygen atom

Table 8
Interaction details of the compounds (**4a,4c,4e,4g-4j**).

Compound	Interactions and amino acids involved											
	Hydrogen Bond	Carbon Hydrogen Bond	Pi-Cation/ Pi-Anion	Pi-Donor Hydrogen Bond	Pi-Sulfur/ Sulfur-X	Alkyl	Pi-Alkyl	Pi-Pi Stacked/ Amide-Pi Stacked	Salt Bridge	Halogen Bond	Pi-Pi T-shaped	Van Der Waals
4a	Gln9	His90, Ser91	His90	Gly8, Ser91	Met131, Phe193, His194	Val189	Leu187, Leu274	–	–	–	His90	Pro7, Ser11, Gln12, Thr54, Val92, Asn155, Asn157, Val163, Arg185, Gly188, Glu267, Pro270, Gly272, Thr273
4c	His90	–	His90	Ser91	–	Val92	Val163, Phe193, His194	–	–	–	–	Pro7, Gly8, Gln9, Gly10, Ser11, Arg116, Met120, Met131, Asn155, Asn157, Leu187, Val189, Glu267, Pro270, Gly272, Thr273, Leu274, Ile277
4e	Gly188	Ser91	His90, Phe193, His194	–	Met131	–	–	–	Arg116	–	–	Gly8, Gly10, Gln12, Thr50, Glu51, Thr54, Ser91, Val92, Met120Arg185, Leu187, Val189
4g	Gln9	–	His90	–	His90	–	Pro7, Leu274	–	Arg185	–	–	Gly8, Gly10, Ser11, Met131, Ala133, Leu135, Asn155, Asn157, Gln161, Leu187, Val189, Phe193, Glu267, Gly272, Thr273, Ile277
4h	–	–	His90	–	His90	Ala59	Met131, Leu187, Val189	Gln9	–	Thr54	–	Pro7, Gly8, Gly10, Ser11, Gln12, Thr56, Ala133, Asn155, Val163, Arg185, Gly188, Glu267, Gly272, Thr273, Leu274
4i	Gly8, Asn155, Thr273	Ser11	His90	–		Met131	Leu187	–	–	–	–	Pro7, Gly8, Gly10, Ser11, Ser91, Val92, Val163, Arg185, Gly188, Val189, Phe193, His194, Val248, Glu267, Thr273, Leu274
4j	–	Gly10, Ser91, Asn157	His90	–	–	Met131, Ile277	Met131	–	–	–	His90	Pro7, Gly8, Gln9, Gly10, Ser11, Ser91, Val92, Arg116, Met120, Asn155, Asn157, Gln161, Leu187, Phe193, His194, Trp250, Gly272 Thr273

"-" corresponds to "No interaction".

from Gln9 can be seen to interact with the hydrogen atom bound to the carbon atom next to the previously mentioned nitrogen atom through carbon-hydrogen bond.

The general structure of compound **4k** differs from the previously discussed compounds. However, it still retains decent binding energy and MIC value. This could be attributed to the numerous interactions provided by the docking results. His90, Ser91 and Asn155 can form hydrogen bonds with the oxygen atom next to the thiazole moiety. Phe193 is involved in pi-alkyl interactions with the 4-Methylthiazole moiety while also stabilizing the ligand via alkyl interaction along with His194 and Leu274. Gly8 is bound to the ligand via carbon-hydrogen bond at two specific hydrogen atoms while Gly10 interacts with the thiadiazole moiety through amide-pi stacked interaction.

The interactions of the other compounds have been described in Table 8. The relatively lower binding energy of compounds **4e** and **4g** could be due to the presence of the partially positively charged nitrogen atom of the nitrobenzene moiety and the presence of positively charged amino acids like His194 and Arg116 in the vicinity leading to steric hindrance.

Interactions have been represented as dashed lines in 2D and 3D representations. In 2D representation, the compounds **4b, 4d, 4f, 4k** are represented as balls and sticks (Fig. 5), and protein amino acids as

Table 9
Summary of the ADMET analysis results.

Molecule	4b	4d	4f	4k	Rifampicin
MW (g/mol)	484.46	435.59	423.55	415.55	822.94
GI absorption	Low	Low	Low	Low	Low
P-gp substrate	No	No	No	No	Yes
CYP1A2 inhibitor	Yes	No	Yes	Yes	No
CYP2C19 inhibitor	Yes	Yes	Yes	Yes	No
CYP2C9 inhibitor	Yes	Yes	Yes	Yes	No
CYP2D6 inhibitor	Yes	Yes	Yes	No	No
CYP3A4 inhibitor	Yes	Yes	Yes	Yes	No
log K_p (cm/s)	−5.42	−5.63	−5.47	−5.99	−7.44
Lipinski rule violations	0	0	0	0	3
Ghose Rule violations	1	0	0	0	3
Veber rule violations	1	2	1	2	1
Egan Rule violations	1	1	1	1	1
Muegge rule violations	2	1	1	1	5
Bioavailability Score	0.55	0.55	0.55	0.55	0.17
PAINS alerts	0	0	0	0	3
Brenk alerts	0	0	0	0	3

spheres. In the 3D representation, compounds **4b, 4d, 4f, 4k** are represented as solid lines and protein amino acids as balls and sticks (Fig. 6).

The protein is rendered as a solid ribbon colored "rainbow" where N terminus is purple and C-terminus is red. The compounds **4b, 4d, 4f, 4k** bound in the active site of MCAT are shown in balls and sticks representation (Fig. 7).

3.5.3. *ADMET study*

As compared to the reference compound Rifampicin, all the compounds demonstrate favorable ADMET profiles suggesting their potential validity for drug development (Table 9). The compounds satisfy Lipinski's rules, show interactions with key enzymes and show suitable bioavailability scores. The compounds display no PAINS and Brenk alerts. PAINS alerts are indicative of presence of substructures which are known to cause false-positive hits during high-throughput screening [53]. Alternatively, Brenk alerts are indicative of unfavorable chemical characteristics such as toxicity, metabolic instability and chemical reactivity [54]. The absence of both PAINS and Brenk alerts hint towards a reduced probability of the compounds causing hindrance in biological assays. Overall, the ADMET results encourage the evaluation of the compounds for further drug developmental studies.

3.5.4. *Toxicity study*

All the compounds fall in the toxicity class "**4**" including the

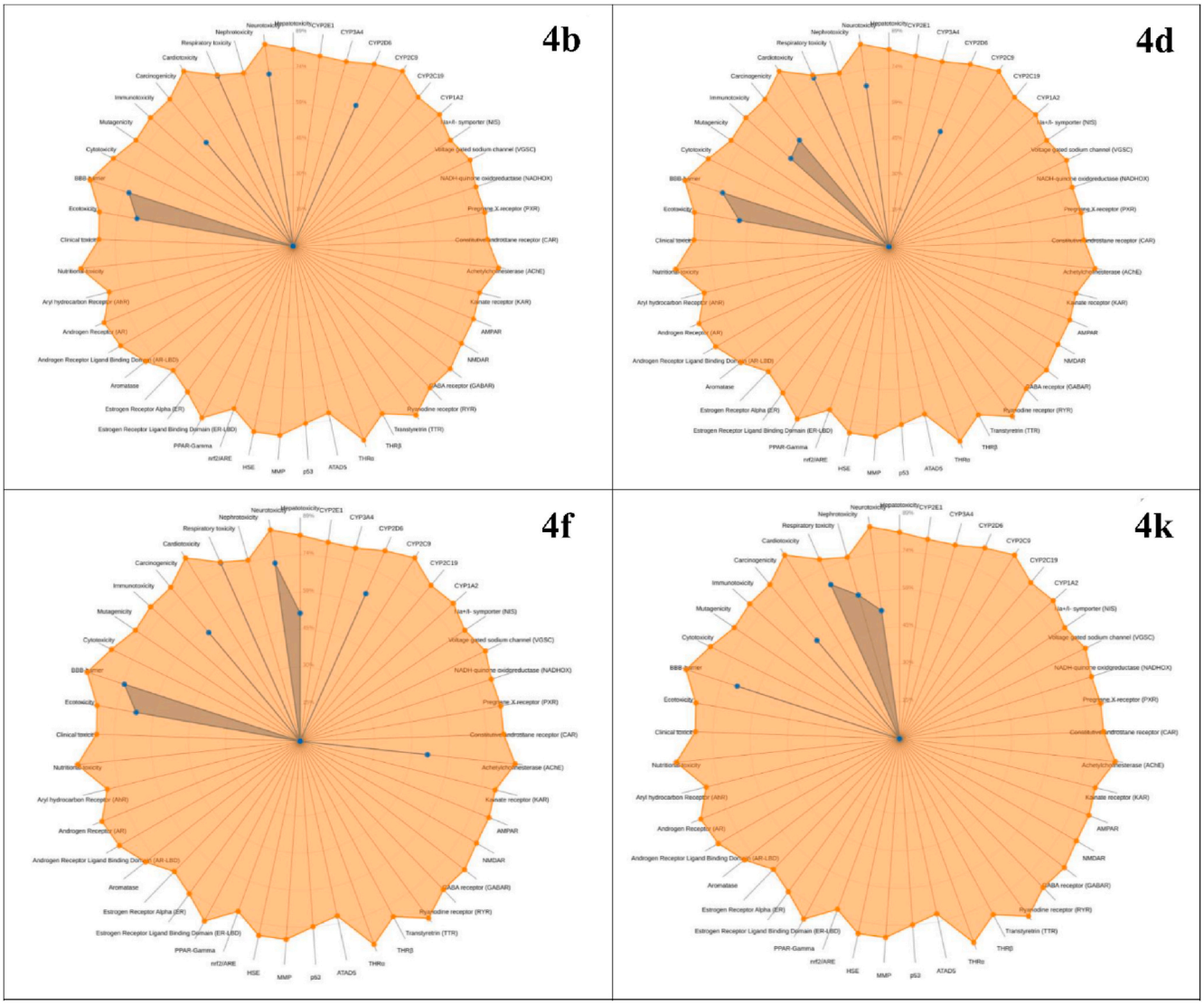

Fig. 8. Toxicity radar charts for compounds **4b, 4d, 4f** and **4k** (Blue: probabilities for activity - user defined molecule Orange: probabilities for activity - average for active molecules). (For interpretation of the references to color in this figure legend, the reader is referred to the Web version of this article.)

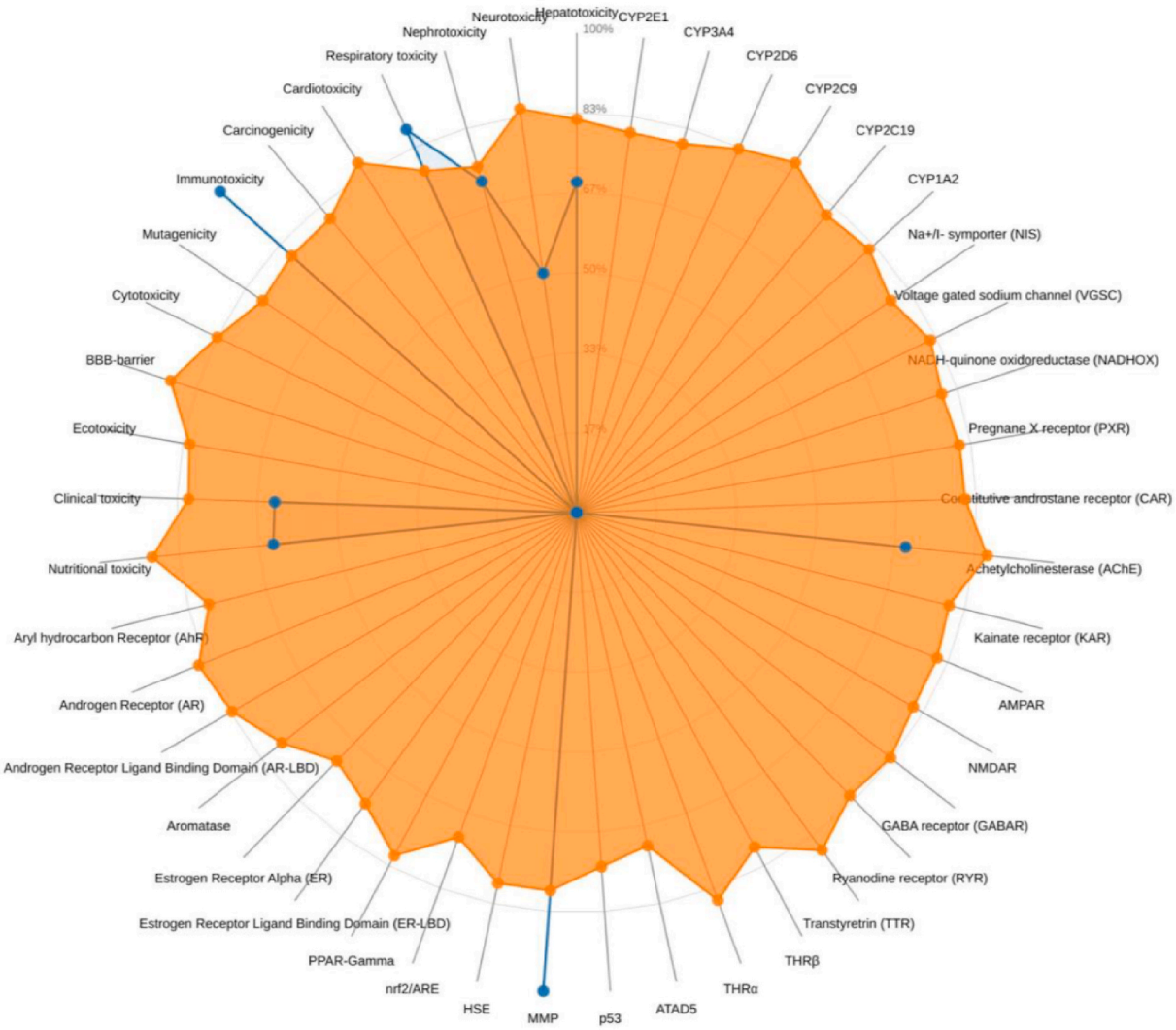

Fig. 9. Toxicity radar chart for reference compound Rifampicin (Blue: probabilities for activity - user defined molecule Orange: probabilities for activity - average for active molecules). (For interpretation of the references to color in this figure legend, the reader is referred to the Web version of this article.)

reference compound Rifampicin, where class **1** is most toxic whereas class **3** is the least toxic. The compounds (**4a-4k**) demonstrated activity in neurotoxicity, respiratory toxicity, carcinogenicity, BBB barrier and ecotoxicity which are indicative towards potential adverse effects on nervous system, respiratory system, risk of cancer development, blood brain barrier integrity and environmental health. By contrast, the compounds demonstrated inactivity in cardiotoxicity, cytotoxicity, nutritional toxicity, clinical toxicity, mutagenicity, nuclear receptor signaling pathways, stress response pathways, molecular signaling events and metabolism suggesting a plausible lack of adverse effects in these areas. The details regarding the toxicological endpoints for each of the compounds as well as the differences observed could be visualized through the toxicity radar charts (Figs. 8 and 9). These results highlight the significance of predictive toxicology in the initial evaluation of the compounds, allowing researchers to leverage the information for activity optimization and lead development process, thereby aiding decision making and risk mitigation.

4. Conclusion

The novel method for the synthesis of thiadiazole-thiazole-acetamide derivatives(**4a-4k**) by using TBAB as catalyst and butylating agent offers high yield with easy product isolation. The structures of the newly synthesized compounds are well confirmed by different spectroscopic techniques such as FT-IR, ^{1}H-NMR, ^{13}C-NMR and MS. DEPT and 2-D techniques as COSY, HETCOR and HMBC confirmed compound **4e**. *In-vitro* antioxidants potential was also explored against DPPH and hydroxyl radicals. The synthesized compounds exhibit moderate to high radical scavenging activities. Importantly, all synthesized compounds and intermediate **3** showed low cytotoxicity towards host RBC compared to Triton X-100. Through a feature-based computational target search, MCAT has been identified as a potential target for the compounds (**4a-4k**). Molecular docking demonstrated binding energy less than 5 kcal/mol for all the compounds (**4a-4k**). Favorable binding energy along with an overall positive correlation of the MIC values and binding energy suggests that MCAT might be the most probable target for these compounds. ADMET and computational toxicology studies suggest the compounds could be suitable for further experimental evaluation considering the comparative results with the standard compound Rifampicin yielded an overall encouraging result.

Ethics approval and consent to participate

We confirm the corresponding author has read the journal policies and submitted this manuscript in accordance with those policies.

Consent for publication

'APPLICABLE'

CRediT authorship contribution statement

Samin A. Shaikh: Writing – original draft, Methodology, Formal analysis, Conceptualization. **Shivaji R. Labhade:** Conceptualization. **Raju R. Kale:** Conceptualization. **Prajakta Y. Pachorkar:** Formal analysis. **Rohan J. Meshram:** Software. **Kamlesh S. Jain:** Methodology. **Hrishikesh S. Labhade:** Conceptualization. **Dipak D. Bhanushali:** Methodology. **Rahul A. More:** Formal analysis. **Charushila K. Nerkar:** Formal analysis. **Santosh S. Chobe:** Investigation. **Aniket N. Marathe:** Visualization, Validation, Conceptualization. **Satish N. Wakchaure:** Data curation. **Deepak R. Boraste:** Writing – original draft.

Declaration of competing interest

We author declare that we have no competing financial interests or personal relationships that could have appeared to influence the work reported in this paper. Please address all correspondence concerning this manuscript to me at samin5577@rediffmail.com or saminshaikh80@gmail.com.

Data availability

The data that has been used is confidential.

Appendix A. Supplementary data

Supplementary data to this article can be found online at https://doi.org/10.1016/j.ejmcr.2024.100183.

References

[1] Lorenzo Guglielmetti, et al., Bedaquiline and delamanid for drug-resistant tuberculosis: a clinician's perspective, Future Microbiol. 15 (9) (2020) 779–799.
[2] Francesca Conradie, et al., Bedaquiline, pretomanid and linezolid for treatment of extensively drug resistant, intolerant or non-responsive multidrug resistant pulmonary tuberculosis, N. Engl. J. Med. 382 (10) (2020) 893.
[3] Vinayak Singh, Chibale Kelly, Strategies to combat multi-drug resistance in tuberculosis, Acc. Chem. Res. 54 (10) (2021) 2361–2376.
[4] Sarah Kim, et al., Evaluating the effect of clofazimine against Mycobacterium tuberculosis given alone or in combination with pretomanid, bedaquiline or linezolid, Int. J. Antimicrob. Agents 59 (2) (2022) 106509.
[5] Sanjeet Bagcchi, WHO's global tuberculosis report 2022, Lancet Microbe 4 (1) (2023) e20.
[6] LİMONCU, HOŞGÖR MİNE, et al., An investigation of the antimicrobial impact of drug combinations against Mycobacterium tuberculosis strains, Turkish J. Med. Sci. 41 (4) (2011) 719–724.
[7] Shaikh, A. Samin, et al., Synthesis, biological evaluation, and molecular docking of novel 1, 3, 4-substituted-thiadiazole derivatives as potential anticancer agent, BMC Chem. 18 (1) (2024) 119.
[8] Samin Anis Shaikh, et al., Synthesis, biological and molecular docking studies of thiazole-thiadiazole derivatives as potential anti-tuberculosis agents, Chem. Biodivers. (2024) e202400496.
[9] Rahul V. Patel, et al., Synthesis of coumarin-based 1, 3, 4-oxadiazol-2ylthio-N-phenyl/benzothiazole acetamides as antimicrobial and antituberculosis agents, Med. Chem. Res. 22 (2013) 195–210.
[10] Aya E. Ghonim, et al., Structure-activity relationships of thiazole and benzothiazole derivatives as selective cannabinoid CB2 agonists with in vivo anti-inflammatory properties, Eur. J. Med. Chem. 180 (2019) 154–170.
[11] Xianghui Ruan, et al., Design, synthesis, and biological activity of novel myricetin derivatives containing amide, thioether, and 1, 3, 4-thiadiazole moieties, Molecules 23 (12) (2018) 3132.
[12] Thoraya A. Farghaly, et al., New and efficient approach for synthesis of novel bioactive [1, 3, 4] thiadiazoles incorporated with 1, 3-thiazole moiety, Eur. J. Med. Chem. 97 (2015) 320–333.
[13] Aamer Saeed, et al., 3-(5-(Benzylideneamino) thiazol-3-yl)-2 H-chromen-2-ones: a new class of alkaline phosphatase and ecto-5′-nucleotidase inhibitors, RSC Adv. 6 (25) (2016) 21026–21036.
[14] Min Zhang, et al., Synthesis and evaluation of 1, 3, 4-thiadiazole derivatives containing cyclopentylpropionamide as potential antibacterial agent, J. Heterocycl. Chem. 56 (7) (2019) 1966–1977.
[15] Eman MH. Abbas, et al., Design, synthesis, cytotoxicity, and molecular docking studies of novel thiazolyl–hydrazone derivatives as histone lysine acetyltransferase inhibitors and apoptosis inducers, Arch. Pharmazie 355 (7) (2022) 2200076.
[16] Mohammad Yusuf, et al., An interactive human carbonic anhydrase-II (h CA-II) receptor–pharmacophore molecular model & anticonvulsant activity of the designed and synthesized 5-amino-1, 3, 4-thiadiazole-2-thiol conjugated imine derivatives, Chem. Biol. Drug Des. 81 (5) (2013) 666–673.
[17] Aram Faraji, et al., Design, synthesis and evaluation of novel thienopyridine-based agents bearing diaryl urea functionality as potential angiogenesis inhibitors, Eur. J. Med. Chem. 209 (2021) 112942.
[18] Dina H. Dawood, et al., Synthesis and molecular docking simulation of new benzimidazole–thiazole hybrids as cholinesterase inhibitors, Arch. Pharmazie 357 (1) (2024) 2300201.
[19] Hyun-Eui Park, et al., Prominent transcriptomic changes in Mycobacterium intracellulare under acidic and oxidative stress, BMC Genom. 25 (1) (2024) 376.
[20] Jin Kyung Kim, Eun-Kyeong Jo, Host and microbial regulation of mitochondrial reactive oxygen species during mycobacterial infections, Mitochondrion (2024) 101852.
[21] El-Refaie Kenawy, et al., Synthesis, characterization and biomedical applications of a novel Schiff base on methyl acrylate-functionalized chitosan bearing p-nitrobenzaldehyde groups, Int. J. Biol. Macromol. 122 (2019) 833–843.
[22] Laura Delvasto-Nuñez, Ilse Jongerius, Sacha Zeerleder, It takes two to thrombosis: hemolysis and complement, Blood Rev. 50 (2021) 100834.
[23] Annuurun Nisa, et al., Different modalities of host cell death and their impact on Mycobacterium tuberculosis infection, Am. J. Physiol. Cell Physiol. 323 (5) (2022) C1444–C1474.
[24] Oguz Özbek, Meliha Burcu Gürdere, Synthesis and anticancer properties of 2-aminothiazole derivatives, Phosphorus, Sulfur, Silicon Relat. Elem. 196 (5) (2021) 444–454.
[25] Husam A. Ameen, Ahlam J. Qasir, Synthesis and preliminary antimicrobial study of 2-amino-5-mercapto-1, 3, 4-thiadiazole derivatives, Iraqi J. Pharmaceut. Sci. (2012) 98–104 (P-ISSN 1683-3597 E-ISSN 2521-3512) 21.1.
[26] Gajanan G. Mandawad, et al., An efficient synthesis of isoxazoline libraries of thiophene analogs and its antimycobacterial investigation, Med. Chem. Res. 23 (2014) 4455–4463.
[27] Shreyas S. Mahurkar, Sangita S. Makone, A. More Rahul, An efficient and recyclable catalyst for synthesis of 1, 3-diphenyl-3-(phenyl thio) propan-1-one derivatives and their antibacterial evaluation, Chem. Biol. Interface 9 (2019) 6.
[28] Rahul More, et al., Antibacterial, antioxidant, phytochemicals evaluation of five Indian medicinal plants, World J. Pharmaceut. Res. 7 (9) (2018) 892–898.
[29] Rahul A. More, et al., Antioxidant and cytotoxicity profile of the selected alcoholic beverages widely consumed in the Maharashtra state of India, Indian J. Publ. Health Res. Dev. 11 (6) (2020) 607–612.
[30] Xiaofeng Liu, et al., PharmMapper server: a web server for potential drug target identification using pharmacophore mapping approach, Nucleic Acids Res. 38 (2010) W609–W614, https://doi.org/10.1093/nar/gkq300. Web Server issue.
[31] Rahul D. Kamble, et al., Synthesis and *in silico* investigation of thiazoles bearing pyrazoles derivatives as anti-inflammatory agents, Comput. Biol. Chem. 61 (2016) 86–96, https://doi.org/10.1016/j.compbiolchem.2016.01.007.
[32] Kapil K. Patil, et al., Role of dietary flavonoids in amelioration of sugar induced cataractogenesis, Arch. Biochem. Biophys. 593 (2016) 1–11, https://doi.org/10.1016/j.abb.2016.01.015.
[33] Pratima P. Mogle, et al., Synthesis and molecular docking studies of a new series of bipyrazol-yl-thiazol-ylidene-hydrazinecarbothioamide derivatives as potential antitubercular agents, MedChemComm 7 (7) (2016) 1405–1420.
[34] S.N. Jangle, Molecular Docking and Binding Energy Studies on Nuraminidase of h1n1 Reveal Possible Answer to its Resistance for Oseltamivir, 2009.
[35] Rohan J. Meshram, et al., Sequence analysis and homology modeling of laccase from Pycnoporus cinnabarinus, Bioinformation 5 (4) (2010) 150.
[36] Rohan J. Meshram, et al., Pharmacophore mapping approach for drug target identification: a chemical synthesis and in silico study on novel thiadiazole compounds, J. Clin. Diagn. Res.: J. Clin. Diagn. Res. 11 (5) (2017) KF01.
[37] Zexuan Li, et al., The crystal structure of MCAT from Mycobacterium tuberculosis reveals three new catalytic models, J. Mol. Biol. 371 (4) (2007) 1075–1083.
[38] Sargis Dallakyan, Arthur J. Olson, Small-molecule library screening by docking with PyRx, Chem. Biol.: Methods Protoc. (2015) 243–250.
[39] Garrett M. Morris, et al., AutoDock4 and AutoDockTools4: automated docking with selective receptor flexibility, J. Comput. Chem. 30 (16) (2009) 2785–2791.
[40] Antoine Daina, Olivier Michielin, Zoete Vincent, SwissADME: a free web tool to evaluate pharmacokinetics, drug-likeness and medicinal chemistry friendliness of small molecules, Sci. Rep. 7 (1) (2017) 42717.
[41] Kyung-Taek Rim, In silico prediction of toxicity and its applications for chemicals at work, Toxicol. Environ. Health Sci. 12 (3) (2020) 191–202.
[42] Priyanka Banerjee, et al., ProTox 3.0: a webserver for the prediction of toxicity of chemicals, Nucleic Acids Res. (2024) gkae303.
[43] A. Kh Khalil, Phase-transfer catalyzed alkylation and cycloalkylation of 2-mercaptoquinazolin-4 (3 H)-One, Phosphorus, Sulfur, and Silicon 180.11 (2005) 2533–2541.
[44] Kalkote Uttam Ramrao, et al., Phase transfer catalyzed N-monoalkylation of amino anthraquinones, Synth. Commun. 21 (10–11) (1991) 1129–1135.
[45] Alvis Brazma, et al., Minimum information about a microarray experiment (MIAME)—toward standards for microarray data, Nat. Genet. 29 (4) (2001) 365–371.

[46] Dario Landini, Michele Penso, A convenient synthesis of N-alkyl and N, N-dialkyltrifluoroacetamides in a solid-liquid two-phase system in the presence of phase-transfer catalysts, Synth. Commun. 18 (8) (1988) 791–800.
[47] Dariusz Bogdal, Fast solvent-free alkylation of amides and lactams under microwave irradiation, Molecules 4 (11) (1999) 333–337.
[48] Ayoub Aghcheli, et al., Design, synthesis, and biological evaluation of 1-(5-(benzylthio)-1, 3, 4-thiadiazol-2-yl)-3-phenyl urea derivatives as anticancer agents, Med. Chem. Res. 29 (2020) 2000–2010.
[49] Jacques Renault, et al., Alkylation of N, N-dibenzylaminoacetonitrile: from five-to seven-membered nitrogen-containing heterocyclic systems, J. Org. Chem. 88 (6) (2023) 3582–3598.
[50] Ekta Verma, Shailendra Patil, Asmita Gajbhiye, Convenient novel method to access N-benzylated isatoic anhydride: reaction behavior of isatoic anhydride with 4-chlorobenzyl chloride in the presence of bases, ACS Omega 6 (12) (2021) 8346–8355.
[51] Acosta Ortiz, Ricardo, et al., Synthesis of a curing agent derived from limonene and the study of its performance to polymerize a biobased epoxy resin using the epoxy/thiol-ene photopolymerization technique, Polymers 14 (11) (2022) 2192.
[52] Laurent Kremer, et al., Biochemical characterization of acyl carrier protein (AcpM) and malonyl-CoA: AcpM transacylase (mtFabD), two major components of Mycobacterium tuberculosis fatty acid synthase II, J. Biol. Chem. 276 (30) (2001) 27967–27974.
[53] Sarah Naomi Bolz, Melissa F. Adasme, Schroeder Michael, Toward an understanding of pan-assay interference compounds and promiscuity: a structural perspective on binding modes, J. Chem. Inf. Model. 61 (5) (2021) 2248–2262.
[54] Chimaobi J. Ononamadu, Ibrahim Aminu, Molecular docking and prediction of ADME/drug-likeness properties of potentially active antidiabetic compounds isolated from aqueous-methanol extracts of Gymnema sylvestre and Combretum micranthum, Biotechnologia 102 (1) (2021) 85.